Direct-to-Earth Communications and Signal Processing for Mars Exploration Rover Entry, Descent, and Landing

E. Satorius,[1] P. Estabrook,[1] J. Wilson,[1] and D. Fort[2]

For planetary lander missions, the most challenging phase of the spacecraft-to-ground communications is during the entry, descent, and landing (EDL). As each 2003 Mars Exploration Rover (MER) enters the Martian atmosphere, it slows dramatically. The extreme acceleration and jerk cause extreme Doppler dynamics on the 8.4-GHz (X-band) signal received on Earth. When the vehicle slows sufficiently, the parachute is deployed, causing almost a step in deceleration. After parachute deployment, the lander is lowered beneath the parachute on a bridle. The swinging motion of the lander imparts high Doppler dynamics on the signal and causes the received signal strength to vary widely due to changing antenna pointing angles. All this time, the vehicle transmits important health and status information that is especially critical if the landing is not successful. Even using the largest Deep Space Network antennas, the weak signal and high dynamics render it impossible to conduct reliable phase-coherent communications. Therefore, a specialized form of frequency-shift keying will be used. This article describes the EDL scenario, the signal conditions, the methods used to detect and frequency track the carrier and to detect the data modulation, and the resulting performance estimates.

I. Introduction

Two Mars rover missions will be launched by NASA in May and June of 2003, during the 2003 Mars launch opportunity. They are the Mars Exploration Rovers, MERA and MERB. The spacecraft will enter the Martian atmosphere directly, without first going into Mars orbit. The rovers will land on the Martian surface in January and February of 2004, in a similar manner to the successful Mars Pathfinder landing in 1996. During the entry, descent, and landing (EDL) phases, it is important to maintain communications from the spacecraft to the Earth. Although this communication cannot affect the landing because the long round-trip light-time precludes real-time feedback from Earth to the spacecraft, the communication could be critical to the success of future missions. This is especially true in case of a mission failure, when the diagnostic data would be very important.

---

[1] Communications Systems and Research Section.

[2] Tracking Systems and Applications Section.

The research described in this publication was carried out by the Jet Propulsion Laboratory, California Institute of Technology, under a contract with the National Aeronautics and Space Administration.

The EDL scenario for MERB is shown in Fig. 1. The scenario for MERA is similar. The rover vehicle is enclosed in a four-sided structure, shaped like a quadrahedron, called the lander. One triangular side is the base, and the other three sides are called petals. After landing, the petals are opened from the base and remain attached to the base. The rover is driven off the lander to conduct its operations. EDL communications is via a direct-to-Earth (DTE) 8.4-GHz (X-band) link, using the backshell low-gain antenna (BLGA). Due to the large dynamic effects encountered during EDL, X-band communication over the DTE link is challenging and requires sophisticated signal processing techniques for reliable demodulation.

In this article, we focus primarily on the signal processing required to demodulate the X-band DTE data tones.[3] We have used, as a point of departure, results from the Mars Pathfinder mission [2]; however, we have extended the signal processing techniques presented in [2] to allow carrier tracking in conjunction with tone demodulation. In the remainder of this article, we first provide a brief overview of MER EDL communications in Section II. We then present details of the DTE communication signal set and the signal detection and tracking techniques in Section III. Analysis and simulation performance estimates are presented in Section IV, data analysis results and implementation losses are discussed in Section V, and a summary is given in Section VI.

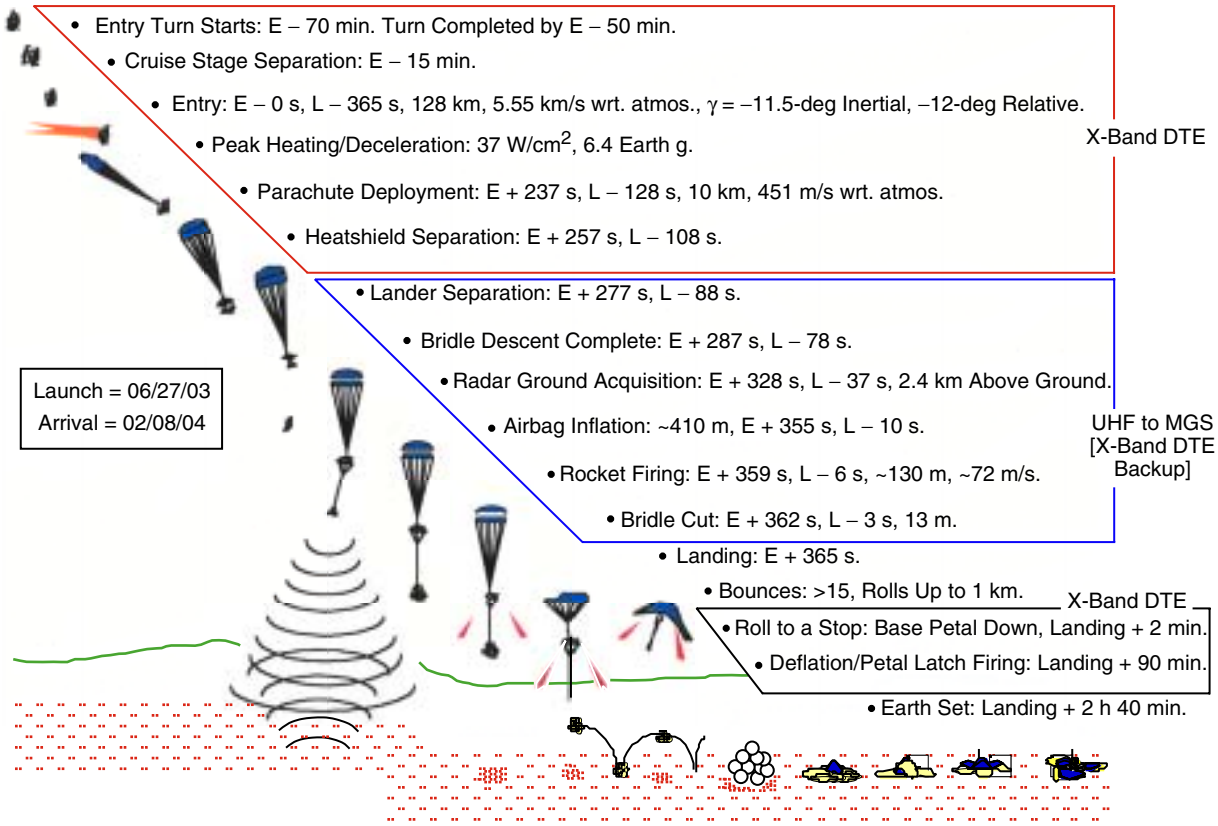

Fig. 1. MERB EDL nominal sequence.

[3] This represents an extension of the material originally presented in [1].

II. MER EDL Communications Overview

From cruise stage separation until the lander is separated from the backshell (see Fig. 1), communication is by a DTE X-band link, using the BLGA. After the lander separates from the backshell, the BLGA can no longer be used. From this point until landing, two methods of communication will be used: a DTE link using the rover low-gain antenna (RLGA) and a UHF relay link. The UHF link transmits the data to either the Mars Odyssey or the Mars Global Surveyor spacecraft, which then relays the data to the Earth using a standard phase-coherent X-band link. After landing, the UHF link will no longer be used, and the DTE link will again be the only link. For purposes of future reference, we somewhat arbitrarily divide EDL into the following stages: (1) cruise (prior to entry); (2) entry (up to approximately 230 s past entry [E+230 s]); (3) parachute deployment (from E+230 s through E+270 s); (4) bridle deployment (E+270 s through E+360 s) and (5) landed (beyond E+360 s).

The X-band DTE link will use a special multiple-frequency-shift-keyed (MFSK) signal format. This has been chosen because the signal conditions of high dynamics and low signal-to-noise ratio (SNR) will not reliably support phase-coherent communications. There will be 256 different signal frequencies, modulated one at a time onto a subcarrier, using the spacecraft capability to switch the subcarrier frequency. During hypersonic entry, the signal frequency can be switched every 10 s, resulting in the communication of 8 bits of information each 10 s. When the lander is suspended from the bridle, and the UHF link is prime, the duration of the modulation frequencies may be extended to 20 s to better facilitate detection during this period of highly varying SNR. This would result in fewer messages of higher reliability than would the use of the 10-s duration.

The expected MERB dynamics profile, magnitude, and uncertainty are illustrated in Fig. 2. The profiles are shown for one of the candidate landing sites. Three different profiles are shown—in green for the nominal entry path angle and in red and blue for other path angles that correspond to the estimated maximum deviations from the nominal profile. For each entry angle, the spacecraft-to-Earth Doppler shift at the X-band frequency is shown in Fig. 2(a). The range of Doppler shift is approximately 90 kHz, and the (two-sided) range of Doppler uncertainty is approximately 50 kHz.

Figure 2(b) shows the Doppler rate, or first derivative of Doppler frequency, due to acceleration. The first maximum occurs due to atmospheric drag during hypersonic entry, at 150 s to 220 s past entry. The maximum varies from 700 Hz/s to 1200 Hz/s, depending on entry angle. The second maximum is a spike in Doppler rate due to parachute deployment. During the hypersonic entry, the range of uncertainty in Doppler rate is roughly the same as the maximum possible Doppler rate. For example, at approximately 150 s past entry, the acceleration could be from approximately 0 Hz/s to 1200 Hz/s. The same is more obviously true for the parachute release. Figure 2(c) shows the second derivative of Doppler frequency due to jerk. During hypersonic entry, the value ranges from approximately -25 Hz/s^2 to 40 Hz/s^2. The exact values shown at parachute deployment are not meaningful due to the inaccuracy in the numerical differentiation used to obtain them.

The SNR for the MERB downlink signal during EDL is shown in Fig. 3. It is the ratio of total power-to-noise spectral density of the X-band signal received at a 70-m DSN antenna. The total power received at the Earth from the spacecraft depends on the angle of the spacecraft with respect to the Earth and on the antenna gain pattern. The antenna gain depends both on the angle off the axis of rotation of the spacecraft and on the rotation angle. The red (center) curve in Fig. 3 is the nominal expected total power SNR versus time. This nominal SNR is based on the spacecraft axis orientation being the nominal angle, and on the nominal antenna gain with respect to rotation angle. The green (upper) curve is the maximum SNR that might be achieved and is based on the most favorable orientation angle, and the blue (lower) curve is the minimum expected SNR. The three vertical dashed lines indicate the nominal times of the key events of parachute deployment at 246 s past entry, lander separation from the backshell at 276 s past entry, and full extension of the bridle with the lander at its end at 286 s past entry.

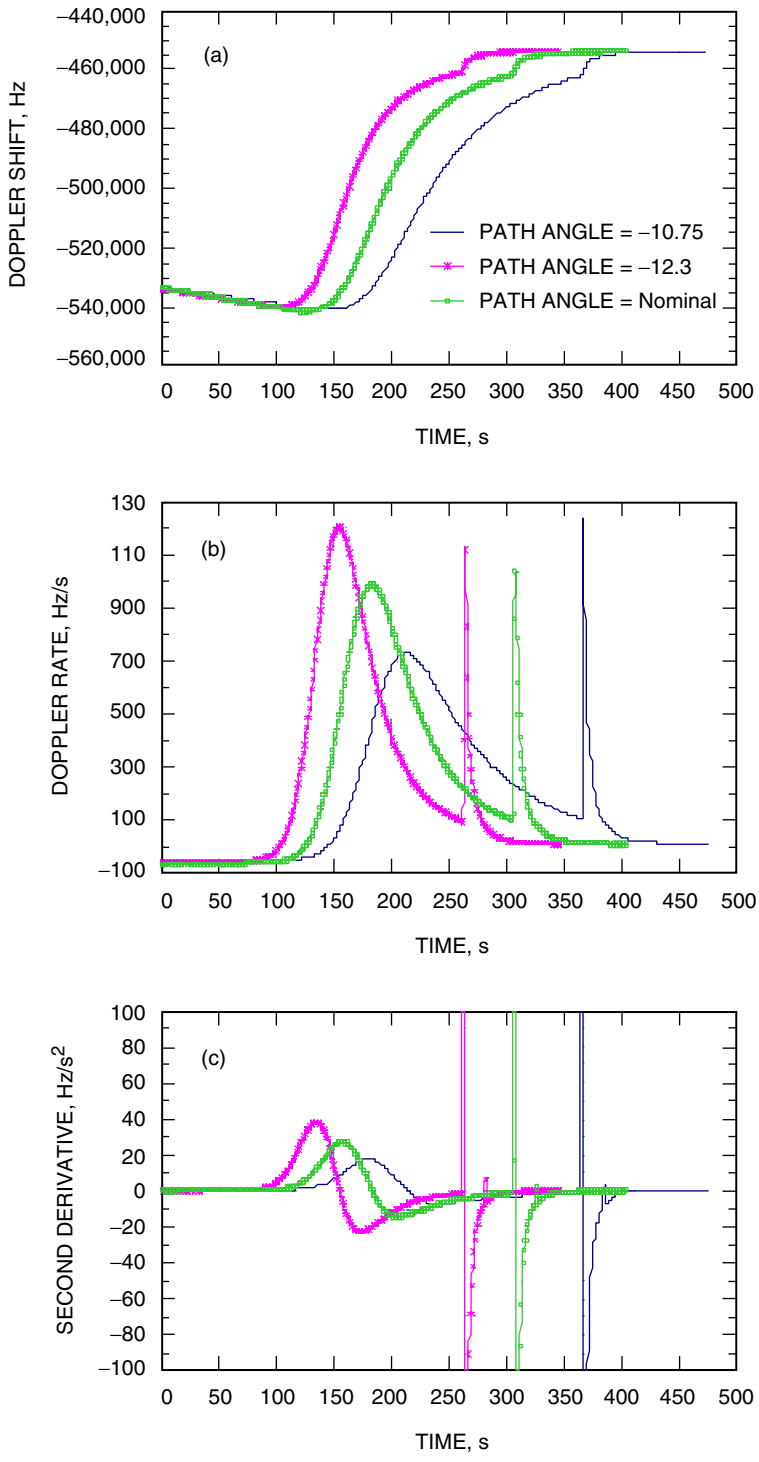

Fig. 2. Doppler dynamics profiles during EDL for nominal, maximum, and minimum flight path angles: (a) Doppler frequency, (b) Doppler frequency rate, and (c) Doppler second derivative.

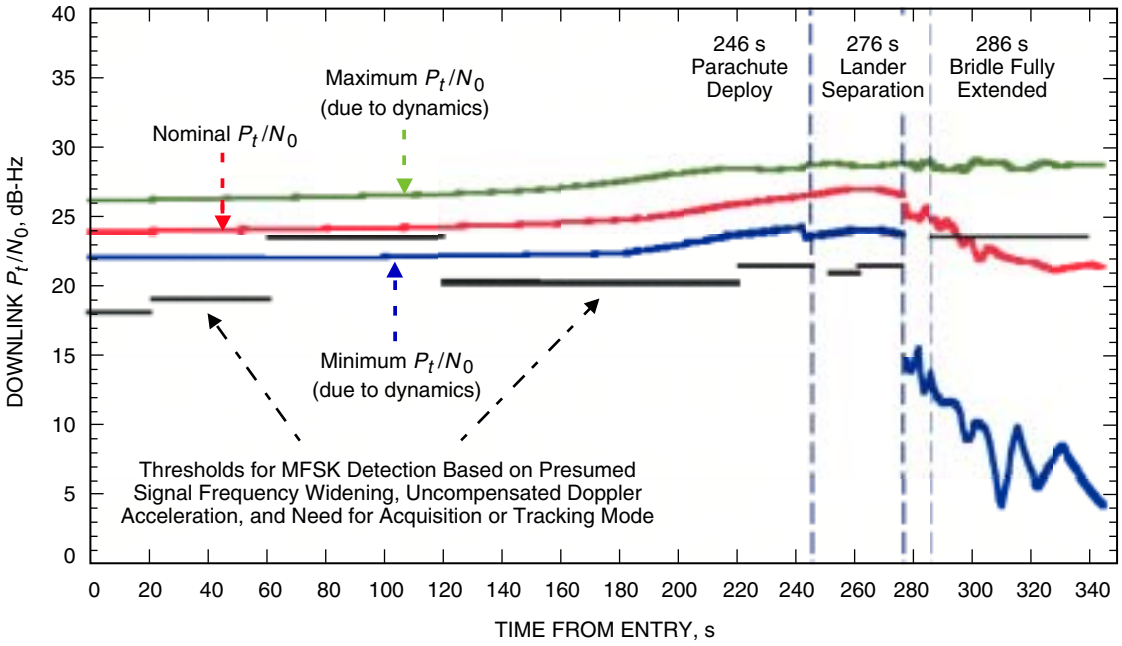

Fig. 3. Signal-to-noise ratio during EDL.

The BLGA is used from entry until lander separation. Throughout this time, the minimum expected SNR is 22 dB-Hz. It is 1 dB to 2 dB higher just before and just after parachute deployment. When the lander is separated from the backshell, the BLGA can no longer be used, and the RLGA is used for the DTE link. The pattern of this antenna is different from that of the BLGA. Also, beginning at this separation, the orientation of the antenna with respect to Earth veers further from the peak antenna gain condition and becomes highly time varying and random. One cause for this behavior is that the attachment point of the bridle to the lander is offset from the spin axis by 15.7 deg, causing the antenna pattern to be offset from the direction to the backshell. Second, the rotational angle of the lander is unknown and is changing on the order of 2 rpm due to spin stabilization of the spacecraft. Finally, the lander will be swinging at the end of the bridle due to the effects of entry and unknown Martian wind. As a result of these effects, the SNR of the signal at the 70-m antenna can vary widely anywhere from 5 dB-Hz to almost 30 dB-Hz as the lander swings and rotates. The black horizontal line segments in Fig. 3 are the estimated SNR thresholds for the various portions of the EDL when using the detection algorithms presented this article. This is discussed in Section V.

During periods of highest dynamics, the combination of low SNR and high dynamics makes reliable phase-coherent communications impossible. For example, use of a type III phase-locked loop (PLL) to track the dynamics would require a loop bandwidth on the order of 13 Hz [3]. The required loop SNR should be approximately 11 dB, which is slightly higher than the 10-dB minimum for coherent communications when there is negligible dynamic phase-lag error. With the 13-Hz loop bandwidth, this results in a required carrier power-to-noise density SNR of 22 dB-Hz. For the lowest SNR profile in Fig. 3, the total power SNR is typically 22 dB-Hz. With half of the total power in the carrier, the carrier SNR would be 3 dB less than the nominal requirement.

Furthermore, a PLL system would have virtually no chance to maintain lock during parachute deployment, and there would not be sufficient time to reacquire lock after deployment in order to receive the important information sent then. There also would be no margin for lower SNR conditions, which are statistically possible. Thus, coherent communication is not feasible and a special form of MFSK will be used, as described in Section III. A major goal of this article is to demonstrate a method of frequency

tracking that will perform satisfactorily throughout the hypersonic entry. It is shown that the SNR tracking threshold for this method is approximately 6 dB better than for a PLL.

For the Mars Pathfinder mission, there was a complete signal outage for approximately 30 s during the period of highest dynamics [2]. Although the cause of this signal loss is not known for sure, it may well have been due to plasma outage [4] and may occur again for the MER missions, depending upon atmospheric conditions during EDL. The frequency-tracking method described in this article is amenable to recovering the signal after loss. The processing will be done non-causally with recorded data. If the signal is lost, the plan is to reacquire it during the period of low dynamics shortly before parachute deployment. The tracking algorithm then will be applied backwards in time, recovering the data back to the end of the signal outage.

It is anticipated that lock will be lost upon parachute deployment. The signal will be reacquired shortly thereafter and processed backwards in time to recover as much data as possible. The final part of the scenario is after the lander is released from the backshell and is suspended on the bridle. The lander is swinging in the wind and rotating due to the spin stabilization of the spacecraft. This causes the antenna gain in the Earth direction to be low, rapidly varying, and poorly predictable, resulting in low and widely varying SNR. During this phase, the UHF relay link is prime, but the X-band DTE data will be processed as best as possible, as a backup. The X-band SNR is expected to vary over a range on the order of 20 dB. There also will be high unmodeled dynamics due to the swinging and rotation of the lander. It is not expected that frequency tracking will be possible. Non-coherent detection algorithms will be used to search over the range of possible Doppler profiles. It is expected that signal detection will be successful when the SNR is at the higher end of its range. It is also expected that some but not all of the frequency-shift keyed (FSK) tones will be detected during this phase. Note that this phase lasts for approximately 80 s, so that there will be only four to eight distinct signals, depending on whether 20-s or 10-s duration tones are transmitted.

III. Signal Set, Detection, and Tracking

The transmitted EDL signal is represented mathematically as

$$s(t) = \sqrt{2P_T}\cos\left\{2\pi \cdot f_c^0 t + \Delta \cdot \mathrm{Sqr}\left(2\pi \int_{-\infty}^{t} d\tau \cdot f_d(\tau)\right)\right\} \tag{1}$$

where P_T is the transmitted power; f_c^0 is the transmitted carrier frequency; Δ is the modulation index ($\cos^2\Delta$ represents the fraction of the total power in the carrier); f_d denotes the data-tone frequency (1 of 256 possible tones transmitted every 10 s); and $\mathrm{Sqr}(\cdot)$ is the hard-limited sine function:

$$\left.\begin{aligned} \mathrm{Sqr}(x) &= \begin{cases} 1, & 0 < x \le \pi \\ -1, & \pi < x \le 2\pi \end{cases} \\ \mathrm{Sqr}(x) &= \mathrm{Sqr}(x + 2\pi) \end{aligned}\right\} \tag{2}$$

Spectrally, $s(t)$ comprises discrete lines at the carrier, data-tone side bands (on either side of the carrier line), and harmonics of the data tone created by the hard-limiting function, $\mathrm{Sqr}(\cdot)$. A sample spectrum of $s(t)$ corresponding to $\Delta = 48$ deg is presented in Fig. 4. As is seen, all data-related spectral components are positioned symmetrically about the carrier line.

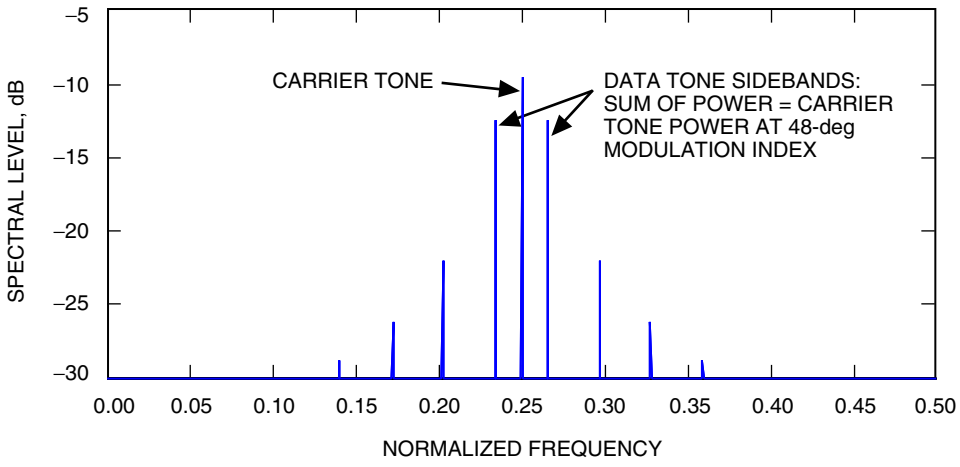

Fig. 4. Sample EDL signal spectrum.

We can express the transmitted carrier and data powers as

$$P_c = P_T \cdot \cos^2 \Delta \tag{3a}$$

and

$$P_d = P_T \cdot \sin^2 \Delta \tag{3b}$$

We can further split the data power P_d into two components: (1) the power in the primary subcarrier, P_{dsc}, and (2) the power in the harmonics, P_{dh}. Thus, $P_d = P_{dsc} + P_{dh}$ or, equivalently, $P_d = P_{dsc} \cdot (1+\rho)$, where $\rho \equiv P_{dh}/P_{dsc} = \pi^2/8 - 1$ is the ratio of harmonic-to-primary subcarrier power. Thus, we have that

$$1 + \rho = \frac{\pi^2}{8} \approx 1.2337 \tag{4}$$

Observe that the transmitted power in the carrier $P_T \cdot \cos^2 \Delta$ matches the power in the primary data subcarrier $P_{dsc} = P_d/(1+\rho) = P_T \cdot \sin^2 \Delta \cdot 8/\pi^2$ when $\Delta \sim 48$ deg. The best choice of Δ represents a trade-off between carrier acquisition/tracking and data-tone detectability. A priori, $\Delta = 48$ deg appears to be a reasonable choice [1]; however, when attempting to reacquire the carrier during EDL phases of high dynamics, a slightly smaller value of Δ may be more appropriate, as will be discussed further in Sections IV and V.

The effect of the communications channel (direct-to-Earth link at X-band) is to introduce significant time-varying amplitude and Doppler (assumed to equally shift the carrier and data subcarrier tones[4]) and to add noise. Thus, we can represent the received signal as

$$x(t) = \sqrt{2P_R(t)} \cos\left\{2\pi \int_{-\infty}^{t} d\tau \cdot f_c(\tau) + \Delta \cdot \mathrm{Sqr}\left(2\pi \int_{-\infty}^{t} d\tau \cdot f_d(\tau)\right)\right\} + n(t) \tag{5}$$

[4] There is a slight (<1-Hz) differential Doppler offset between the carrier and the largest primary data subcarrier offset frequency (the maximum subcarrier offset frequency is ∼15 kHz), but this typically is negligible compared to the nominal carrier-tracking resolution bandwidth—especially during periods of high dynamics.

where P_R denotes the generally time-varying total received signal power—it is assumed that the relationships in Eqs. (3) and (4) also apply to the portioning of P_R into the received carrier and data powers. The received carrier frequency can be represented as the sum of the transmitted frequency and a time-varying Doppler component $\Delta f(t)$, i.e., $f_c(t) = f_c^0 + \Delta f(t)$. In detecting and demodulating this waveform, the carrier frequency, $f_c(t)$; its time derivative, $\dot{f}_c(t)$ (frequency rate); and, in certain cases of high dynamics, its second time derivative, $\ddot{f}_c(t)$ (frequency acceleration), first are tracked out via a fast Fourier transform (FFT)-based maximum-likelihood detection approach [5]. The transmitted MFSK data tones then are determined.

The carrier-acquisition process is essentially an open-loop search over carrier frequency and rate space wherein different hypothesized rates are first mixed out of a segment of the input data,[5] i.e.,

$$r_\ell(t) \equiv x(t) \cdot \exp\left\{-2\pi j\left(\hat{\dot{f}}_c^\ell(t) \cdot \frac{t^2}{2}\right)\right\} \quad 0 \le t \le T; 1 \le \ell \le N_r \tag{6}$$

where $\hat{\dot{f}}_c^\ell(t)$ denotes the ℓth hypothesized carrier frequency rate (N_r possible rates) and T is the time span of the segment. Each segment $r_\ell(t)$ is further sub-divided into M contiguous subsegments of duration $\Delta T = T/M$. FFTs of each sub-segment then are computed ($N_{FFT} \equiv F_s \cdot \Delta T$ points per FFT, where F_s denotes the sampling rate and $\Delta f = F_s/N_{FFT}$ is the frequency resolution of the FFT) and the magnitude-squared FFTs for each ℓth rate are averaged together to form the periodogram estimates $P_\ell(f_k)$, $1 \le \ell \le N_r$; $f_k \equiv (k/\Delta T)([-N_{FFT}/2] + 1 \le k \le [N_{FFT}/2])$. Initial estimates of the carrier frequency and rate are derived via

$$\left.\begin{matrix}\hat{f}_k \\ \hat{\dot{f}}_\ell\end{matrix}\right\} = \arg\max_{\ell, f_k}\{P_\ell(f_k)\} \tag{7}$$

The resulting estimates, $\hat{f}_c(0) \equiv \hat{f}_k$ and $\hat{\dot{f}}_c(0) \equiv \hat{\dot{f}}_\ell$, then are used to initialize carrier-frequency tracking. This is similar to the acquisition process except that carrier frequency, rate, and (possibly) acceleration estimates derived from a T-length data segment are used as initial estimates for the next segment, and so on. For tracking, these segments typically are overlapped (50 to 75 percent overlapping) in order to provide smoother frequency estimates to the data-tone demodulator and also to minimize large frequency excursions between estimates. In addition, the sizes of the frequency and frequency rate spaces are substantially reduced during tracking. A simplified block diagram of the EDL signal processor is presented in Fig. 5(a),[6] and the carrier-tracking process is depicted in Fig. 5(b).

Based on dynamics considerations[7] as well as the above discussion, we summarize in Table 1 nominal EDL signal processing parameters and search ranges (frequency, frequency rate) used for the five stages of EDL defined above: cruise, entry, parachute deployment, bridle deployment, and landed. The signal processing parameters are based on a $F_s = 100$-kHz sampling rate. The tracking update rate relates to the window overlapping used during tracking, i.e., $\delta\tau$ in Fig. 5(b). Typically, $\delta\tau \sim (T/2)$, as noted above, except in the landed phase, when $(\delta\tau/T) < 0.1$ in order to provide smooth frequency estimates required for tone demodulation under low signal-to-noise ratio conditions (see Fig. 3).

---

[5] Typically, searching over frequency accelerations is reserved for the carrier-tracking phases.

[6] In general, a larger number of processing states can be used in addition to the acquisition and tracking states [8].

[7] The dynamics considerations are as presented in E. Satorius and C. Racho, "EDL Signal Threshold Assessment and Signal Processing Considerations," presented at the Peer Review of MER X-Band Communications During EDL (internal document), Jet Propulsion Laboratory, Pasadena, California, June 11, 2001.

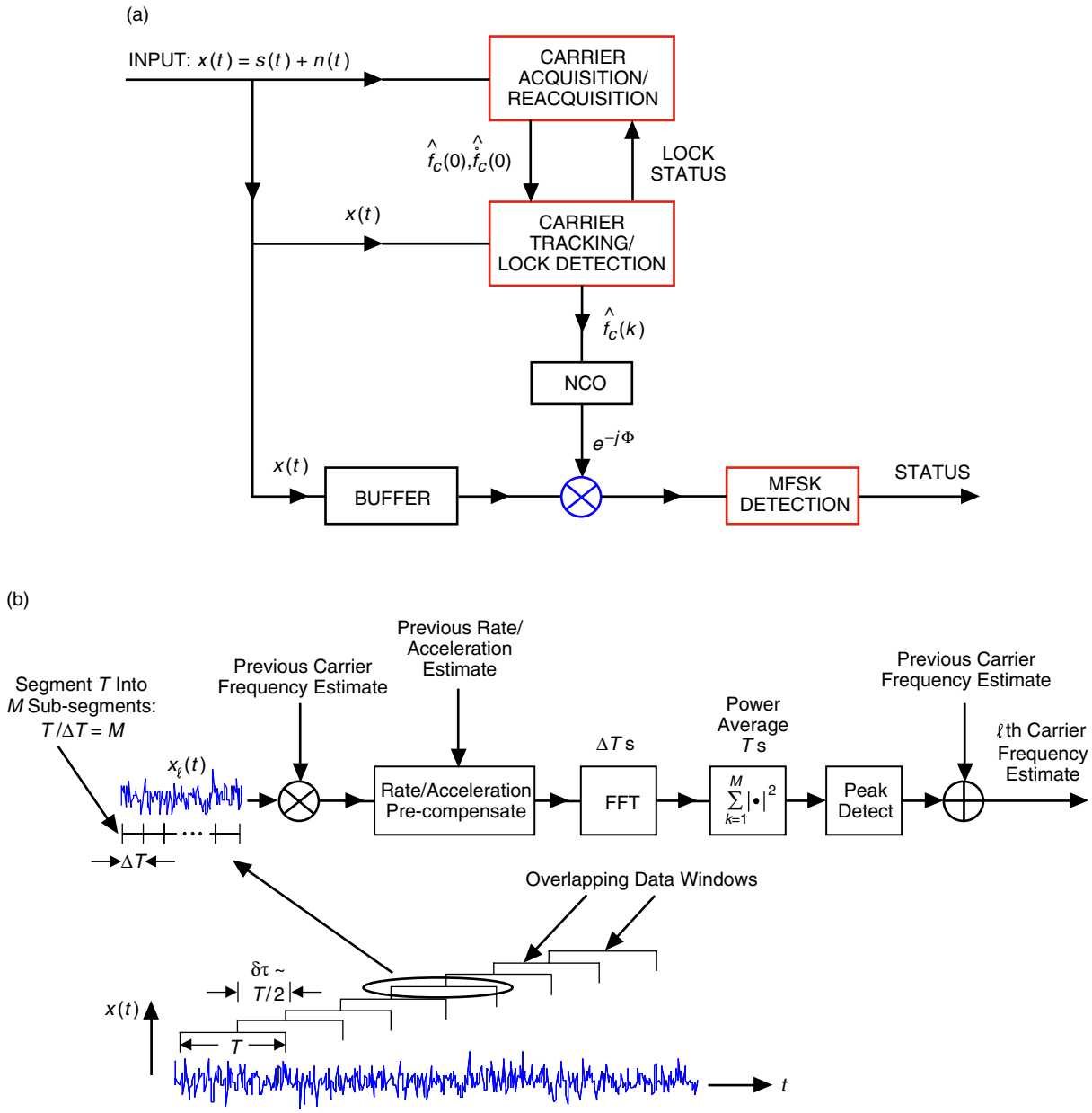

Fig. 5. EDL signal processing: (a) block diagram of the EDL signal processor and (b) the EDL tracking process.

Note that during the high dynamics stages of EDL (entry, parachute deployment, and bridle deployment), the detection interval T used for carrier tracking and acquisition is nominally 1 s (2 s in the lower dynamics, cruise stage). However, during the landed stage when the dynamics are very low, a much longer interval can be used ($T \sim 15$ s) and in fact is desirable due to the potentially lower signal-to-noise ratio conditions. On the other hand, the tone-detection interval typically is matched to the symbol duration (nominally 10 s, possibly longer during the landed stage) since the effects of carrier dynamics have been removed to a large extent by the carrier tracker.

As indicated in Table 1, the FFT resolution used for carrier tracking and acquisition typically is between 5 and 20 Hz during the cruise, entry, parachute deployment, and bridle deployment stages in order to accommodate the higher dynamics during these stages. Similarly, the FFT resolution used

for tone detection during these higher dynamics stages is on the order of 10 Hz, reflecting the greater frequency uncertainty in the carrier-frequency estimates. However, during the low dynamics, landed stage, the FFT resolutions used for both carrier tracking/acquisition and tone detection are nominally 1 Hz.

Finally, we note in Table 1 that the carrier-frequency and frequency-rate search ranges are substantially reduced in the transition from acquisition to tracking (the frequency acceleration search space is even smaller during tracking, if it is used, and thus is not included in Table 1). This results in a lower carrier-tracking threshold (approximately 2 to 3 dB lower) due to the reduction in the size of the search space (thereby reducing the probability of false carrier detection).

Table 1. Nominal EDL signal processing parameters and search ranges.

Parameter	Cruise	Entry	Parachute	Bridle deploy	Landed
FFT frequency resolution, Δf, used for tracking/ acquisition	5 to 10 Hz ($N_{FFT} = 20,000$ to 10,000)	20 Hz ($N_{FFT} = 5,000$)	10 Hz ($N_{FFT} = 10,000$)	20 Hz ($N_{FFT} = 5,000$)	1 Hz ($N_{FFT} = 100,000$)
Tracking update rate	0.5 s	0.5 s	0.5 s	0.5 s	1 s
Frequency search range	−200 Hz to 200 Hz (tracking) −25 kHz to 25 kHz (acquisition)	−200 Hz to 200 Hz (tracking) 100 kHz (acquisition)	−200 Hz to 200 Hz (tracking) 100 kHz (acquisition)	−200 Hz to 200 Hz (tracking) −15 kHz to 15 kHz (acquisition)	−50 Hz to 50 Hz (tracking) −5 kHz to 5 kHz (acquisition)
Frequency rate resolution	1.25 Hz/s (tracking) 10 Hz/s (acquisition)	5 Hz/s (tracking) 80 Hz/s (acquisition)	3.333 Hz/s (tracking) 30 Hz/s (acquisition)	5 Hz/s (tracking) 10 Hz/s (acquisition)	0.02 Hz/s (tracking and acquisition)
Frequency rate search range	−7.5 Hz/s to 7.5 Hz/s (tracking) −100 Hz/s to 100 Hz/s (acquisition)	−20 Hz/s to 20 Hz/s (tracking) −800 Hz/s to 800 Hz/s (acquisition)	−13.33 Hz/s to 13.33 Hz/s (tracking) −300 Hz/s to 300 Hz/s (acquisition)	−20 Hz/s to 20 Hz/s (tracking) −100 Hz/s to 100 Hz/s (acquisition)	−0.02 Hz/s to 0.02 Hz/s (tracking and acquisition)
Detection interval, T, used in tracking/acquisition	2 s	1 s	1.5 s	1 s	15 s
FFT frequency resolution for tone detection, Δf	5 Hz	10 Hz	10 Hz	10 Hz	1 Hz
Detection interval, T, used for tone detection	10 s	10 s	10 s	10 s	10 to 30 s

IV. Performance Analysis

From a performance analysis standpoint, carrier tracking is considered to be the same as acquisition except that the size of the search space is drastically reduced and, thus, the tracking threshold is usually somewhat lower (approximately 1 to 2 dB lower) than for acquisition. Likewise, MFSK tone detection is based on peak power estimation except that Doppler rate is eliminated from the search space and, furthermore, the number of frequencies searched is reduced to the number of possible MKSK tones. Thus, since acquisition normally sets the overall detection threshold, we focus first on EDL acquisition of the carrier.

In deriving EDL receiver acquisition performance estimates, several critical assumptions are made. First, we note that regardless of whether we are performing carrier acquisition, tracking, or MFSK tone detection, the estimation process always is based on peak power detection. In the case of carrier acquisition, the maximum over all possible frequencies and rates is determined as the initial estimate of the carrier frequency. We denote the size of the search space (the number of Doppler N_{FFT} and Doppler rate N_r pairs) by $N_f \equiv N_{FFT} \cdot N_r$ and assume that the correct carrier signal is present in only 1 of the N_f search locations. Denote the carrier Doppler frequency by f_{ks} and the Doppler rate by $\hat{f}_{\ell s}$.

It is further assumed that, over the detection interval T, the received carrier frequency trajectory is linear, and thus the effects of high-order frequency dynamics, i.e., frequency acceleration and above, are neglected (incorporation of frequency acceleration estimates is reserved for carrier tracking). Finally, it is assumed that the periodogram data $P_\ell(f_k)$ can be characterized statistically as N_f independently distributed random variables. Initially, it is assumed that the powers in the data harmonic components as well as the primary data subcarriers are negligible compared with the average noise power in each frequency and rate cell. In this case, the $P_\ell(f_k)$ are characterized by the following two distributions:

(1) $P_\ell(f_k)$ is central chi-square with $2M$ degrees of freedom ($M = T\Delta f$) provided ℓ does not coincide with the carrier Doppler rate index ($\ell \neq \ell s$) and/or provided that f_k does not coincide with the carrier Doppler frequency index ($f_k \neq f_{ks}$).

(2) If $\ell = \ell s$ and $f_k = f_{ks}$, $P_\ell(f_k)$ is non-central chi-square with $2M$ degrees of freedom and the non-centrality parameter: $\lambda \equiv 2 \cdot T \cdot CNR \equiv 2 \cdot T \cdot P_R NR \cdot \cos^2 \Delta$, where CNR is the received carrier power-to-noise density ratio and $P_R NR$ denotes the ratio of the total received power (carrier plus data)-to-noise density (recall from Eq. (3) that the ratio of carrier power to the total power is $\cos^2 \Delta$)[8].

The carrier is correctly acquired provided its associated energy, $P_{\ell s}(f_{ks})$, is the largest of all the Doppler–Doppler rate cells *and* provided $P_{\ell s}(f_{ks})$ exceeds a threshold, V_T. Given the above distributions for $P_\ell(f_k)$, items (1) and (2), the probability of correct carrier acquisition, P_{acq}, can be expressed as

$$P_{acq} = \int_{V_T}^{\infty} dx \cdot F_Y(x) \cdot f_S(x) \tag{8a}$$

where [6,7]

$$f_S(x) = \frac{1}{2} \left(\frac{x}{\lambda} \right)^{(M-1)/2} e^{-(x+\lambda)/2} I_{M-1} \left(\sqrt{\lambda x} \right) \tag{8b}$$

and

[8] Here it is assumed that the total received power P_R is constant, at least over the total detection interval, T.

$$\left.\begin{aligned} F_Y(x) &= \left(\int_0^x du \cdot f_n(u)\right)^{N_f-1} \\ f_n(x) &= \frac{x^{M-1} \cdot e^{-x/2}}{2^M \cdot (M-1)!} \end{aligned}\right\} \tag{8c}$$

In Eq. (8b), $I_{M-1}(\cdot)$ is the modified Bessel function of the first kind and of order $M-1$, and the noncentrality parameter, $\lambda = 2 \cdot T \cdot CNR$, is equivalent to twice the received carrier signal energy-to-noise spectral density ratio. The carrier-acquisition threshold V_T can be directly related to the false alarm probability P_{FA} (probability of detecting a noise peak instead of the carrier) via

$$P_{FA} = 1 - \left(\int_0^{V_T} du \cdot f_n(u)\right)^{NM} \tag{8d}$$

Thus, given P_{FA}, V_T can be obtained by inverting Eq. (8d). Substituting Eqs. (8b) through (8d) into Eq. (8a) yields the desired relationship for the probability of correct carrier acquisition in terms of the various detection parameters: M; T; P_RNR; Δ; $N_f \equiv N_{FFT} \cdot N_r$; and P_{FA}. Note that, if we let P_{FA} approach 1, the carrier-acquisition threshold V_T approaches 0. In this limit, a detection threshold is not used, and the Doppler–Doppler rate cell with the largest energy over the carrier-acquisition search space is taken to be the carrier signal cell. Plots of $1 - P_{acq}$ versus $CNR = P_RNR \cdot \cos^2 \Delta$ corresponding to $P_{FA} = 0.0001, 0.01, 0.1$, and 1.0 (i.e., $V_T = 0$ corresponding to no thresholding) are provided in Fig. 6. The other detection parameters were set at $M = 10$, $T = 1$ s, and $N_f = 570,000$, corresponding to coarse frequency rate acquisition under high dynamics conditions, e.g., using a $\Delta f = 10$ Hz FFT resolution searching over a 100-kHz bandwidth and over a 1400-Hz/s frequency rate space in steps of 25 Hz/s (representative of the parameters in Table 1).

As is seen, the probability of missed carrier acquisition is much higher at $P_{FA} = 10^{-4}$ and 10^{-2} due to the lack of threshold crossings of $P_{\ell s}(f_{ks})$. For example, at $CNR = 15.5$ dB-Hz, the missed detection probability when setting the threshold to zero is approximately 7 percent, which means that about 93 percent of the time the peak detections indeed coincide with the carrier frequency. However, it must be noted that the 7 percent missed detections are noise spikes and further processing of these

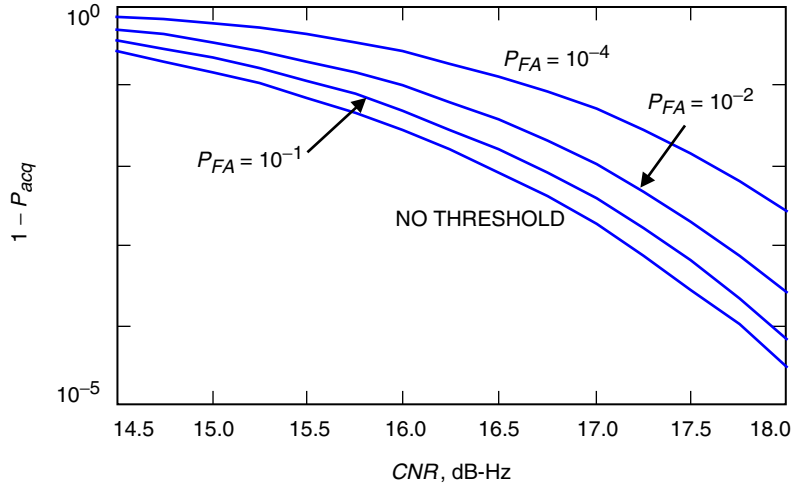

Fig. 6. Probability of missed carrier acquisition with and without noise thresholding.

spikes will simply waste processing time and resources. On the other hand, examining the $P_{FA} = 10^{-2}$ curve in Fig. 6 reveals that the missed detection probability is a much higher 21 percent. However, the majority of these missed detections occur when the peak detections do not exceed the threshold V_T. In these cases, no valid detection is made. Only 1 percent of the peak detections due to noise will actually exceed the threshold at $P_{FA} = 10^{-2}$, thereby reducing wasted processing time.

Nevertheless, of the 21 percent missed detections at $P_{FA} = 10^{-2}$, about 67 percent are valid carrier signal detections.[9] Consequently, we have adopted the strategy of using very little or no thresholding during carrier acquisition to reduce the number of missed carrier detections (when the peak detection coincides with the carrier frequency). Time wasted on processing false peaks can be recovered during post (refined) processing. Thus, in the following, a zero detection level is assumed.

Equation (8a) provides an optimum bound on EDL carrier-acquisition performance since the effects of the data tones and higher-order dynamics (frequency acceleration and above) have been neglected. The inclusion of the data tones in this analysis (still neglecting higher-order dynamics) is straightforward based on the following assumptions:

(1) First and foremost, it is assumed that no special processing is used to distinguish detected data tones from the actual carrier as used, for example, in Pham and Fort.[10] In this sense, the results presented here represent worst-case performance estimates.

(2) $P_\ell(f_k)$ is central chi-square with $2M$ degrees of freedom provided ℓ does not coincide with the carrier Doppler rate index ($\ell \neq \ell s$) and/or provided that f_k does not coincide with either the carrier Doppler frequency index ($f_k \neq f_{ks}$) or one of the primary data subcarrier frequencies (we assume that the powers in the data harmonic components are negligible compared to the noise—see Fig. 4).

(3) If $\ell = \ell s$ and f_k coincides with one of the primary data subcarrier frequencies, $P_\ell(f_k)$ is non-central chi-square with $2M$ degrees of freedom and the non-centrality parameter: $\lambda_d \equiv 2 \cdot T \cdot \{\sin^2 \Delta \cdot P_R NR \cdot 8/\pi^2\}/2$ (recall from Eq. (3) that the ratio of transmitted data power to the total transmitted power is $\sin^2 \Delta$ and that the ratio of data power to the sum of power in both the primary data subcarriers is $\pi^2/8$—as noted above [Eq. (5)], it is assumed that this relationship also holds for the received signal).

(4) If $\ell = \ell s$ and $f_k = f_{ks}$, $P_\ell(f_k)$ is non-central chi-square with $2M$ degrees of freedom and the non-centrality parameter: $\lambda_c \equiv 2 \cdot T \cdot P_R NR \cdot \cos^2 \Delta$.

To compute the probability of correct carrier acquisition, we use the same formulation as above [Eq. (8)], except that Eq. (8c) is modified to include the primary data subcarrier frequencies, i.e.,

$$F_Y(x) = \left(\int_0^x du \cdot f_n(u) \right)^{N_f - 3} \cdot \left(F_{dt}(x) \right)^2 \tag{9}$$

where $f_n(x)$ is defined in Eq. (8c) and $F_{dt}(x)$ is the non-central chi-square distribution with $2M$ degrees of freedom and the non-centrality parameter $\lambda_d \equiv 2 \cdot T \cdot \{\sin^2 \Delta \cdot P_R NR \cdot 8/\pi^2\}/2$ (primary data subcarriers). The corresponding density function $f_{dt}(x) = dF_{dt}(x)/dx$ is given by [6,7]

---

[9] Corresponding to 93 percent (with no thresholding) less 79 percent correct detections with thresholding divided by 21 percent total missed detections at $P_{FA} = 10^{-2}$, i.e., $(93 - 79)/21 \sim 67$ percent.

[10] T. Pham and D. Fort, "EDA Requirements and Design," JPL presentation to EDL personnel (internal document), Jet Propulsion Laboratory, Pasadena, California, March 1, 2002.

$$f_{dt}(x) = \frac{1}{2}\left(\frac{x}{\lambda_d}\right)^{(M-1)/2} e^{-(x+\lambda_d)/2} I_{M-1}\left(\sqrt{\lambda_d x}\right) \tag{10}$$

The density function of $P_\ell(f_k)$ at the carrier frequency ($\ell = \ell s$ and $f_k = f_{ks}$) is given by Eq. (8b) with $\lambda_c \equiv 2 \cdot T \cdot P_R NR \cdot \cos^2 \Delta$. Substituting Eqs. (8b) and (9) with Eq. (8c), Eq. (10) into Eq. (8a) (with $V_T = 0$, as discussed above) yields the desired relationship for the probability of correct carrier acquisition in the presence of the primary data subcarriers as a function of the various detection/modulation parameters: M; T; $P_R NR$; $N_f \equiv N_{FFT} \cdot N_r$; and Δ.

We can now compute the carrier-acquisition probability as a function of $P_R NR$. Consider a high-dynamics, high rate-resolution carrier-acquisition scenario wherein the FFT resolution is again set at $\Delta f = 10$ Hz; the non-coherent FFT averaging duration is $T = 1$ s; the frequency search space is 100-kHz wide; and the frequency rate search space is 1400-Hz/s wide in steps of 2.5 Hz/s.[11] Plots of the corresponding probability of incorrect carrier acquisition ($1 - P_{acq}$) versus $P_R NR$ with and without the primary data subcarriers taken into account and for $\Delta = 45$ and 48 deg are presented in Fig. 7. As is seen, this small, 3-deg decrease in the modulation index results in a significant reduction in carrier-acquisition threshold in the presence of the data tones. For example, the threshold (with data tones) reduces by more than 2 dB at $P_{acq} = 0.99$ and by approximately 2.5 dB at $P_{acq} = 0.999$. Ignoring the data tones in the analysis would predict a much smaller improvement ($\sim$0.5 dB) in acquisition threshold.

This substantial reduction in carrier-acquisition threshold is a consequence of the increase in received carrier power and simultaneous decrease in the primary data subcarrier power. This is illustrated in Fig. 8, where plots of $P_c/P_T = \cos^2 \Delta$ [Eq. (3)] and $P_{dsc}/P_T = \sin^2 \Delta \cdot 8/\pi^2$ [Eqs. (3) and (4)] are presented as a function of Δ (again it is assumed this same power distribution holds for the received signal). As is seen,

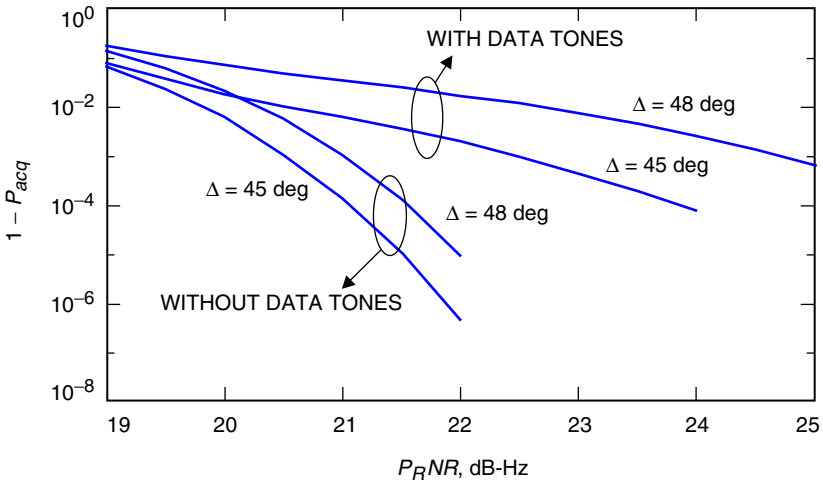

Fig. 7. Probability of incorrect carrier acquisition.

[11] Thus, $N_f = 5,610,000$ for this open-loop acquisition search. The specific value of N_f has a greater impact on the carrier-acquisition probability when the data tones are not included in the analysis [Eq. (8)]. This is due to their strong influence on the incorrect carrier detections [Eq. (9)]—especially as $P_R NR$ increases. For example, additional calculations reveal that the carrier-acquisition error probability is approximately constant as N_f decreases by a factor of 10 from 5,610,000 to 561,000 when the data tones are included in the analysis and $P_R NR$ is at least 20 dB-Hz. When they are not included, the required value of $P_R NR$ to maintain a given carrier-acquisition error probability decreases by approximately 0.5 dB, e.g., at $1 - P_{acq} \sim 0.02$, the required value of $P_R NR$ is 20 dB-Hz when $N_f = 5,610,000$ but reduces to 19.6 dB-Hz as N_f is decreased by a factor of 10.

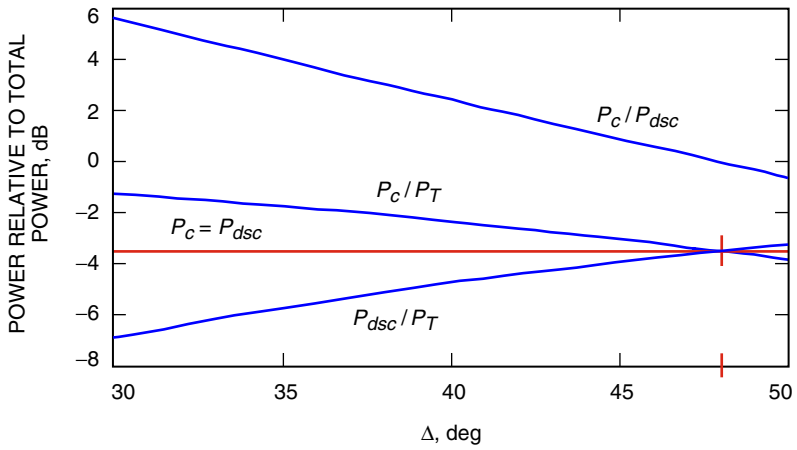

Fig. 8. Distribution of power between the carrier, P_c, and primary data subcarrier, P_{dsc}.

lowering the modulation index by only 3 deg from 48 to 45 deg increases the carrier-to-data subcarrier power ratio by approximately 1 dB, thereby leading to the reduction in carrier-acquisition threshold, as noted above.

The corresponding reduction in the data subcarrier power has considerably less impact on data-tone detectability. Specifically, the probability of correct data-tone detection, P_{sym}, is given by

$$P_{sym} = \int_0^\infty dx \cdot F_{Y\,sym}(x) \cdot f_{fdt}(x) \tag{11a}$$

where

$$f_{fdt}(x) = \frac{1}{2}\left(\frac{x}{\lambda_{dsym}}\right)^{(2M-1)/2} e^{-(x+\lambda_{dsym})/2} I_{2M-1}\left(\sqrt{\lambda_{dsym} x}\right) \tag{11b}$$

and

$$\left.\begin{aligned} F_{Y\,sym}(x) &= \left(\int_0^x du \cdot f_{nsym}(u)\right)^{N_{sym}-1} \\ f_{nsym}(x) &= \frac{x^{2M-1} \cdot e^{-x/2}}{2^{2M} \cdot (2M-1)!} \end{aligned}\right\} \tag{11c}$$

In Eq. (11b), $\lambda_{dsym} \equiv 4 \cdot T_{sym}\{\sin^2 \Delta \cdot P_R NR \cdot [8/\pi^2]\}/2$ is the non-centrality parameter for the data tone (T_{sym} typically is matched to the symbol duration, 10 s, but can be shorter with some loss in performance), and in Eq. (11c), $N_{sym} = 256$ represents the total number of possible data tones transmitted. Comparing Eq. (11b) with Eq. (10) and Eq. (11c) with Eq. (8c) reveals that M has been replaced with $2M$. This is a consequence of spectral folding about the carrier prior to data-tone detection.

Plots of the symbol-error probability, $1 - P_{sym}$, as a function of $P_R NR$ are presented in Fig. 9 for $\Delta = 45$ deg and 48 deg. These plots correspond to $N_{sym} = 256$, $T_{sym} = 10$ s, and a $\Delta f = 10$-Hz

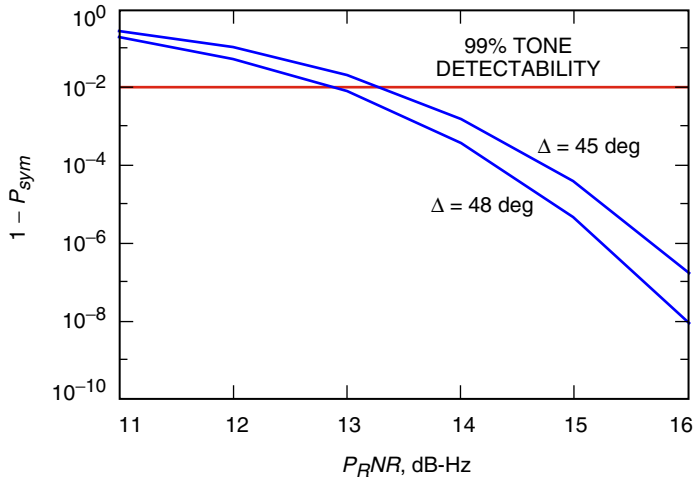

Fig. 9. Data-tone error probability.

FFT resolution (thus, in this case $M = T_{sym} \cdot \Delta f = 100$). These tone-detection parameters would be appropriate under high-dynamics conditions wherein the carrier-frequency uncertainty is on the order of 5 to 10 Hz, matching the FFT resolution used for carrier acquisition (Fig. 7). As is seen, 99 percent tone detectability (a goal for EDL) is achieved at $P_R NR \sim 13$ dB-Hz when $\Delta = 48$ deg. This increases only by approximately 0.25 dB at $\Delta = 45$ deg.

However, the point is that to achieve this level of tone detectability (99 percent), the carrier first must be acquired. We can express the total probability of tone detection, P_{tone}, as

$$P_{\text{tone}} = P_{acq} \cdot P_{sym} + \frac{(1 - P_{acq})}{N_{sym}} \tag{12}$$

where again $N_{sym} = 256$ for EDL. If $P_{sym} \sim 0.99$, then P_{acq} must approach 0.999 so that $P_{\text{tone}} \sim 0.99$. Assuming P_{acq} is between 0.99 and 0.999, we see from Fig. 7 that if, for example, $P_{acq} = 0.99$, then $P_R NR$ must exceed 20.5 dB-Hz if $\Delta = 45$ deg (22.5 dB-Hz if $\Delta = 48$ deg). With reference to Fig. 9, it is seen from the standpoint of tone detectability that the choice of Δ (45 or 48 deg) is immaterial at such a high $P_R NR$. In any case, $P_{sym} \sim 1.0$ when $P_R NR$ exceeds approximately 14 dB-Hz. Even during carrier tracking (under high-dynamics conditions), the threshold is typically in excess of 17 dB-Hz, in which case again the choice of Δ (45 or 48 deg) is irrelevant insofar as tone detectability is concerned.

Additional calculations of P_{acq} and P_{sym} at $\Delta = 40$ deg reveal that the carrier-acquisition threshold at $P_{acq} = 0.99$ is approximately $P_R NR = 19.2$ dB-Hz, whereas $P_{sym} \sim 1.0$ once $P_R NR$ exceeds 16 dB-Hz. Given that the carrier-tracking threshold at $P_{acq} = 0.99$ (and $\Delta = 40$ deg) will be in excess of 16 dB-Hz, we propose that a modulation index between 40 and 45 deg be used during periods of highest dynamics (at least through bridle swinging—see Fig. 1). This conclusion is further supported by experimental measurements of carrier-tracking errors at different modulation indices (Section V.C).

After landing, the situation is considerably different since the signal is relatively stable. Thus, a much smaller FFT resolution ($\Delta f \sim 1$ Hz) in combination with a much longer detection interval ($T > 10$ s) can be used to acquire and track the carrier. In this case, there is much less distinction between the carrier acquisition/tracking and tone-detection thresholds. Therefore, an equal split of the power between the carrier and the primary data subcarriers is reasonable, and thus it is recommended that the modulation index be increased to $\Delta = 48$ deg after landing.

As an example of EDL tracking performance, we have simulated the MERB frequency profile (see Fig. 2) and impressed it upon the transmitted carrier. Simulated tracking performance at $P_RNR = 19.4$ dB-Hz and $\Delta = 48$ deg is presented in Fig. 10(a). Utilizing a 10-Hz FFT resolution and a $T = 0.7$-s detection interval, we are able to continuously track the carrier through periods of peak dynamics all the way up to parachute deployment (the track depicted in Fig. 10(a) was terminated just prior to parachute deployment). Note also from Fig. 10(a) that the root-mean-square (rms) frequency-tracking error σ_f is approximately 1.5 Hz (in general $\sigma_f \propto \Delta f$). This is more than adequate for reliable MFSK tone detection, as illustrated in Fig. 10(b), where a waterfall display of the detected 10-s MFSK tones over time is depicted (approximately 23 tones transmitted from entry to parachute deployment). As is seen, there is plenty of margin for correctly demodulating all of the data tones. Finally, we note that at $P_RNR = 19.4$ dB-Hz and $\Delta = 48$ deg the carrier SNR is approximately 16 dB-Hz, which is indeed 6 dB below the carrier-tracking threshold of a type III PLL, as discussed in Section II.

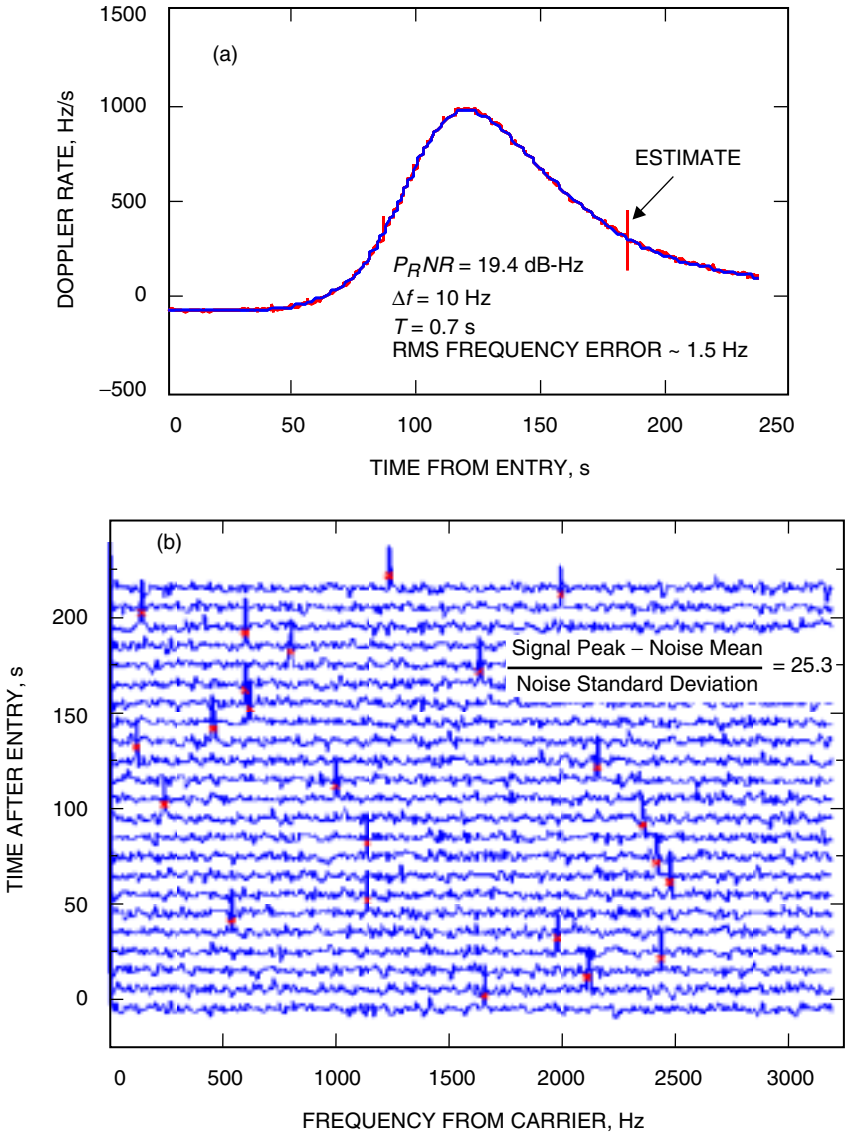

Fig. 10. Simulated MERB EDL processor performance: (a) tracking and (b) tone detection.

V. Data Analysis Results and Implementation Losses

Data collected from three separate series of MER MFSK tests have been processed with the EDL signal processor depicted in Fig. 5. The first series of tests was conducted September 10–12, 2001, at Data Tracking Facility (DTF-21)[12] and comprised data collections at low P_RNR ($\leq$10 dB-Hz) and high P_RNR ($\geq$19 dB-Hz). The modulation index for these collections was nominally set at $\Delta = 48$ deg, and the simulated dynamics varied from approximately static (reflecting the landed EDL stage) to a carrier-frequency profile representative of a typical EDL scenario up to and including the bridle deployment stage. In addition, two tests from the first series used a periodic carrier-frequency profile with a constant frequency acceleration of 20 Hz/s^2 to simulate carrier acquisition, tracking, and tone demodulation under conditions of high dynamics. Selected processing results from this first series of tests are presented in Section V.A.

The second series of tests was conducted November 26–30, 2001, at DTF-21[13] and comprised data collections at low P_RNR ($\leq$9.5 dB-Hz) and high P_RNR ($\geq$17 dB-Hz). The modulation index for these collections also was set at $\Delta = 48$ deg, and the simulated dynamics once again varied from approximately static (reflecting the landed EDL stage) to a carrier-frequency profile representative of a typical EDL scenario up to and including the bridle-deployment stage. In addition, tests at varying P_RNR (22 dB-Hz down to 17 dB-Hz) used a periodic carrier-frequency profile with a constant frequency acceleration of 20 Hz/s^2 to simulate carrier acquisition, tracking, and tone demodulation under conditions of high dynamics and at different P_RNR. Special tests also were carried out in this second series to simulate preempted data tones and assess their impact on data-tone demodulation. Selected processing results from this second series of tests are presented in Section V.B.

Finally, a third series of tests was conducted March 15–19, 2002, at DTF-21[14] for the purposes of (1) testing carrier tracking/tone detection at very low P_RNR (between 6 and 8 dB-Hz), (2) testing EDL processing performance with different modulation indices (between 40 and 48 deg), and (3) testing the engineering EDL data analysis software [15] on entire simulated EDL runs (from the cruise stage through entry, descent, and landing). The tests conducted with different modulation indices, item (2) above, used both the periodic carrier-frequency profile with a constant frequency acceleration of 20 Hz/s^2 at a P_RNR varying between 16.5 and 22 dB-Hz and a low-frequency (0.1-Hz) sinusoidal frequency profile with P_RNR varying between 6 and 21 dB-Hz (to simulate swinging on the bridle). Selected processing results from these tests are presented in Section V.C.

A. Selected Processing Results from the First Series of EDL Tests

We first present the results of carrier-acquisition processing of the Test 8 data set. For Test 8, a simulated EDL signal was generated and recorded in complex baseband format at a 100-kHz sample rate. The signal comprised a carrier (periodic frequency variation between approximately $\pm$10 kHz, corresponding to a constant 20-Hz/s^2 frequency acceleration) and 5-s subcarrier data tones. The modulation index was held constant at 48 deg. The nominal simulated P_RNR was 22 dB-Hz, and the test duration was approximately 10^4 s (almost 3 h). A wideband (100-kHz-wide) carrier-acquisition search over approximately one-fourth the data set (about 2500 s) was carried out with the following search parameters: T = 1-s detection interval; Δf = 10-Hz FFT frequency resolution (10,000 frequency cells); and rates from $-$700 Hz/s to 700 Hz/s in steps of 2.5 Hz/s (561 total rates).

---

[12] P. Estabrook, "Mars Exploration Rover M-FSK Testing Plan for TDL/DTF-21 Tests," internal document, Jet Propulsion Laboratory, Pasadena, California, September 10, 2001.

[13] P. Estabrook, "Mars Exploration Rover M-FSK Testing Plan for TDL/DTF-21 Tests," internal document, Jet Propulsion Laboratory, Pasadena, California, November 26, 2001.

[14] P. Estabrook, "Mars Exploration Rover M-FSK Testing Plan for TDL/DTF-21 Tests on RFS#2," internal document, Jet Propulsion Laboratory, Pasadena, California, March 13, 2002.

[15] T. Pham and D. Fort, op cit.

Thus, $N_f = 5,610,000$ for this search, corresponding to that used in generating the curves in Fig. 7. The measured probability of incorrect carrier acquisition over the 2500-s data segment was found to be approximately 0.045.[16] A plot of the resulting open-loop carrier-frequency estimates (a representative 950-s subsegment) is presented in Fig. 11(a). Based on the average peak carrier amplitudes as well as the average background spectral noise level, the ratio of carrier power-to-noise spectral density CNR was estimated to be approximately 18.2 dB-Hz. Given that the Test 8 data were generated with a 48-deg modulation index, we infer that $P_RNR = CNR/\cos^2\Delta \sim 21.7$ dB-Hz, which is slightly less than the planned P_RNR of 22 dB-Hz.[17]

Careful inspection of Fig. 7 reveals that an error rate of 0.045 is achieved at $P_{tot}NR \sim 20.7$ dB-Hz (corresponding to the curve with data tones and a 48-deg modulation index). Thus, the carrier-acquisition error results from Test 8 are about 1 dB worse than theory. To understand the source of this implementation loss, a 950-s segment of 100-kHz data (carrier plus 5-s data tones at a 48-deg modulation index) was synthesized, corresponding to $P_{tot}NR = 21.7$ dB-Hz and with frequency dynamics

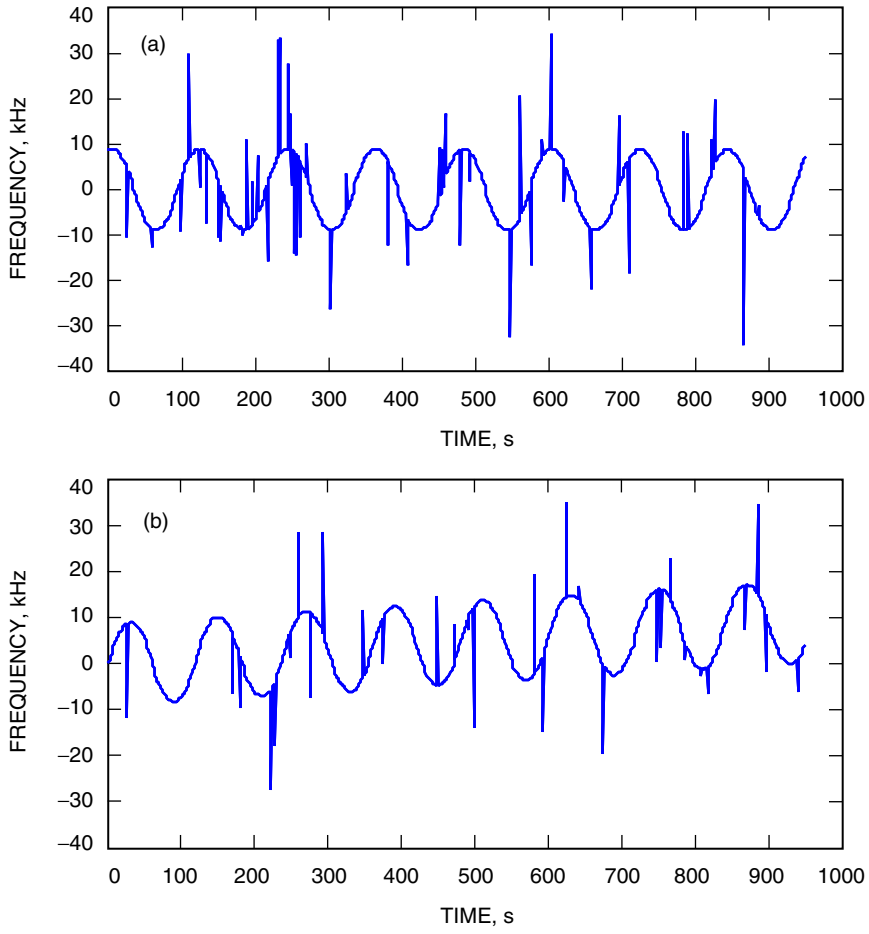

Fig. 11. Open-loop carrier-frequency estimates: (a) from Test 8 and (b) with synthesized carrier-plus-data tones (48-deg modulation index) at P_RNR = 21.7 dB-Hz.

[16] Carrier-acquisition errors were declared whenever the carrier estimate deviated by at least an FFT resolution cell from the actual carrier-frequency profile, which was known for this test.

[17] P. Estabrook, September 10, 2001, op cit.

approximately matched to the Test 8 data set.[18] A plot of the resulting open-loop carrier-frequency estimates is presented in Fig. 11(b). These estimates were obtained using the same acquisition search parameters as used for Test 8. The carrier-frequency error rate for the 950-s synthesized data set was found to be 0.032. From Fig. 7, this is achieved at $P_R NR \sim 21.2$ dB-Hz, indicating a 0.5-dB loss with the synthesized data.

To understand the statistical significance of the observed difference in the measured carrier-acquisition error probabilities (0.045 for Test 8 and 0.032 for the synthesized data set), it is noted that the number of errors out of N independent tests has a binomial probability distribution given by

$$\text{Probability}\{k \text{ errors out of } N \text{ tests}\} \equiv P_e(k|N) = \frac{N!(1-P_{acq})^k P_{acq}^{N-k}}{k!(N-k)!} \tag{13}$$

The mean number of errors and associated standard deviation are given by

$$\left.\begin{aligned} \bar{k} &= (1-P_{acq}) \cdot N \\ \sigma_k &\equiv \sqrt{\overline{k^2} - \bar{k}^2} = \sqrt{(1-P_{acq}) \cdot P_{acq} \cdot N} \end{aligned}\right\} \tag{14}$$

The estimate of the carrier-acquisition error probability is simply k/N and, thus, its standard deviation is $\sqrt{(1-P_{acq}) \cdot P_{acq}}/\sqrt{N}$. From Fig. 7 (the curve with data tones and a 48-deg modulation index), it is seen that the theoretical carrier-acquisition error probability at $P_R NR = 21.7$ dB-Hz is approximately 0.022. Substituting this into Eq. (14) with $N = 950$ (matching the length of the synthesized data set), it is seen that the acquisition-error probability estimate derived from the synthesized data (0.032) lies more than 2 standard deviations from the theoretical probability. The probability of this occurrence is only about 4 percent.[19] Furthermore, the 0.045 error probability observed in Test 8 (derived from $N = 2500$ independent tests) lies almost 8 standard deviations from the theoretical probability.

From this we can conclude (1) there is a statistically significant residual loss in carrier-acquisition performance beyond the degradation imposed by the presence of the primary data tones and (2) there may be additional loss between the Test 8 and synthesized data sets, e.g., due to inaccurate knowledge of the various parameters ($P_{tot}NR$, Δ) or perhaps to unmodeled dynamics. In an attempt to identify the source of the observed residual loss in carrier-acquisition performance, an independent 800-s segment of 100-kHz data (carrier plus 5-s data tones at a 48-deg modulation index) was synthesized again, corresponding to $P_R NR = 21.7$ dB-Hz. However, for this test, the carrier and data-tone frequencies were static over time and, thus, the effects of frequency dynamics were removed from the corresponding data analysis.

A plot of the resulting open-loop carrier-frequency estimates is presented in Fig. 12. The carrier-frequency error rate for this synthesized data set is approximately 0.018,[20] which is well within a standard deviation of the theoretical result, $1 - P_{acq} \sim 0.022$. Thus, we may conclude that frequency dynamics represent a significant source for the added loss in carrier-acquisition performance (beyond that imposed by the presence of the primary data tones). Based on the above results, we can estimate this added loss to be between 0.5 and 1 dB.

---

[18] Note that a linear frequency drift is present in the synthesized data [Fig. 11(b)] as compared to Test 8 [Fig. 11(a)]. Nevertheless, this does not invalidate the basic findings presented here.

[19] For large N, $P_e(k|N)$ [Eq. (13)] is approximately normally distributed. The probability that the carrier-acquisition error-probability estimate, k/N, is greater than 3 standard deviations away from the true probability, $1 - P_{acq}$, is only about 0.3 percent. At 2 standard deviations, this increases to 4.5 percent, and at 1 standard deviation this is almost 32 percent.

[20] It should be noted that the frequency errors occurring in Fig. 12 all coincided with the primary data subcarrier frequencies.

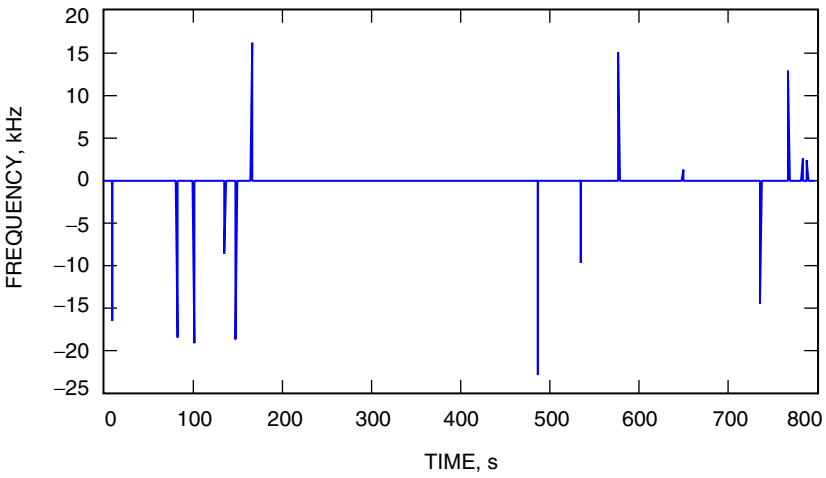

Fig. 12. Open-loop carrier-frequency estimates with synthesized carrier-plus-data tones (48-deg modulation index) at P_RNR = 21.7 dB-Hz but with static carrier and data-tone frequencies.

Finally, to examine the influence of the modulation index on EDL carrier-acquisition performance, an independent 950-s segment of 100-kHz data was simulated with the same parameters as used before [Fig. 11(b)] *except* that the modulation index was decreased from 48 to 45 deg. The resulting open-loop carrier-frequency estimates are plotted in Fig. 13. Comparing Figs. 11(b) and 13, the dramatic improvement in carrier-acquisition performance is clearly observed. The carrier-frequency error rate for this 950-s synthesized data set was found to be approximately 0.0053 and, as in the case of Fig. 12 (see Footnote 20), all of the carrier errors coincided with the primary data subcarrier frequencies.

The theoretical result (Fig. 7 curve with data tones and a 45-deg modulation index) is approximately 0.0028. Substituting this into Eq. (14) with $N = 950$, it is seen that the acquisition-error probability estimate derived from the synthesized data (0.0053) falls well within 2 standard deviations of the theoretical probability. The probability of this occurrence is about 13 percent. Thus, not only is there a significant improvement in acquisition performance by reducing the modulation index to 45 deg, this also appears to slightly lessen the added loss due to frequency dynamics. Experimental results at a 45-deg modulation index are presented and discussed in Section V.C.

In addition to carrier-acquisition testing, two tone-detection tests were conducted under nominally static carrier-frequency conditions (with the exception of slow oscillator drifts) and low P_RNR conditions. For both tests, the signal comprised the carrier and 10-s subcarrier data tones. The modulation index was held constant at 48 deg. The first of these tests, Test 4, was again approximately 10^4 s (almost 3 h) in duration, and the nominal (planned) P_RNR was 10.5 dB-Hz. Given the low dynamics and low P_RNR, the carrier was tracked with the following parameters for Test 4: T = 10-s detection interval (carrier estimates output at a 1-Hz rate to facilitate tone demodulation); Δf = 1-Hz FFT frequency resolution (100,000 frequency cells); and three frequency rates searched, 0 Hz/s and ±0.05 Hz/s.

A plot of the tracked carrier for a segment of Test 4 is provided in Fig. 14. A slow carrier drift is clearly observed on the order of −0.02 Hz/s, which falls well within the frequency-rate search range (±0.05 Hz/s). Based on the average peak carrier amplitudes as well as the average background spectral noise level, the ratio of carrier power-to-noise spectral density CNR was estimated to be approximately 7.5 dB-Hz. This is about 0.5 dB larger than the planned $CNR = P_RNR \cdot \cos^2 \Delta \sim 7$ dB-Hz.

In addition to carrier tracking, the tones also were demodulated using the following parameters: T = 10-s detection interval and Δf = 1-Hz FFT frequency resolution. These parameters correspond to $M = T\Delta f = 10$ in Eq. (11). Furthermore, given that 1 of 256 possible tones was transmitted every

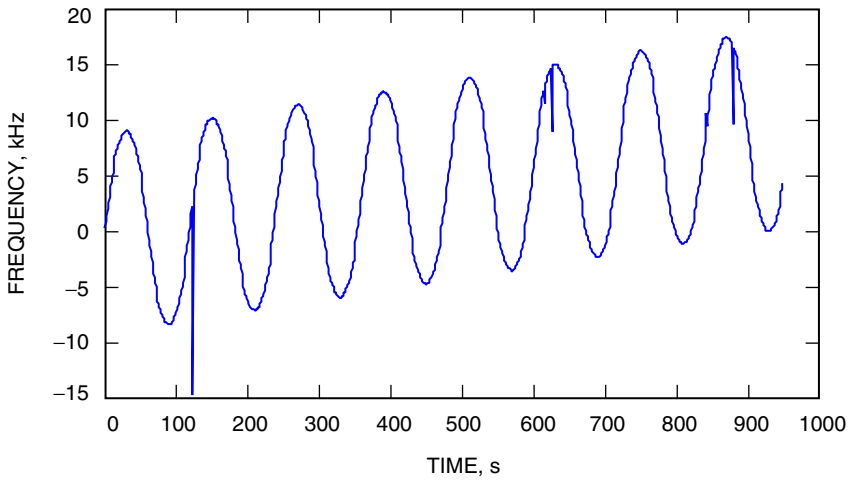

Fig. 13. Open-loop carrier-frequency estimates with synthesized carrier-plus-data tones (48-deg modulation index) at P_RNR = 21.7 dB-Hz with frequency dynamics approximately matched to the Test 8 data set (see Footnote 18).

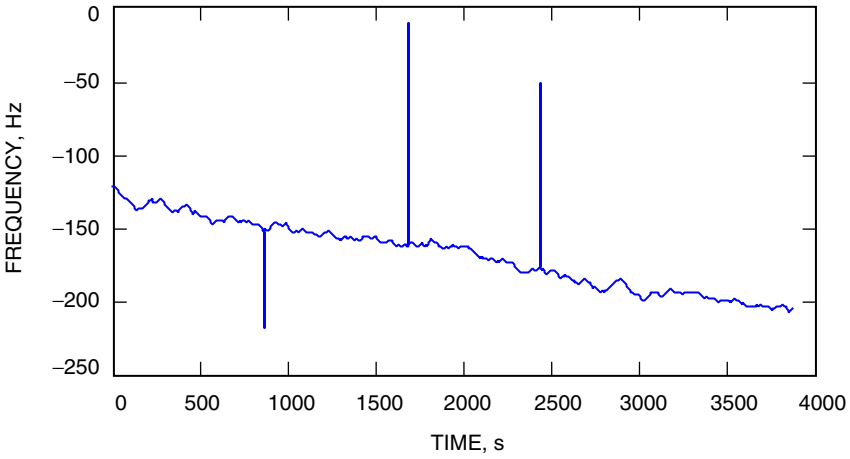

Fig. 14. Carrier-tracking estimates for Test 4.

10 s (100-Hz separation between tone frequencies), the search space was restricted to the 256 possible tone locations, i.e., $N_{sym} = 256$ in Eq. (11). The corresponding plot of data-tone error probability $1 - P_{sym}$ versus P_RNR is provided in Fig. 15. It should be noted that in demodulating the tones, as depicted in Fig. 5(a), an initial segment comprising typically 10 to 20 data tones first is processed to obtain the boundaries for tone detection (i.e., tone synchronization). All of the tones then are demodulated over these tone boundaries (without re-synching).

Based on the average detected tone power as well as the average background spectral noise level, the ratio of tone power (in the primary subcarriers)-to-noise spectral density was estimated to be approximately 7.8 dB-Hz. This is about 0.8 dB larger than the planned $\sin^2\Delta \cdot P_RNR \cdot 8/\pi^2 \sim 7$ dB-Hz. Thus, given the above CNR estimate of 7.5 dB-Hz for Test 4 as well as the 7.8 dB-Hz estimate for the ratio of tone power-to-noise spectral density, we estimate P_RNR for Test 4 to be approximately 11.1 dB-Hz—0.6 dB higher than planned.

Out of a total of 1004 transmitted tones in Test 4, only 13 were incorrectly demodulated, corresponding to a measured tone-error probability of $1 - P_{sym} \sim 0.013$. With reference to Fig. 15, we see that

theoretically a tone-error probability of 0.013 can be achieved at $P_RNR \sim 8.9$ dB-Hz, thus implying an implementation loss of $11.1 - 8.9 = 2.2$ dB. On the other hand, we would expect theoretically a tone-error probability of $1 - P_{sym} \sim 0.00002$ at $P_RNR = 11.1$ dB-Hz (Fig. 15). Substituting this into Eq. (14) with $N = 1004$ (and replacing P_{acq} with P_{sym}), it is seen that the tone-error probability estimate (0.013) falls well outside the standard deviation of the theoretical probability ($\sim 1.4 \cdot 10^{-4}$). Thus, the 2.2-dB implementation loss in tone-detection performance observed in Test 4 is statistically significant and is due, in part, to carrier-tracking errors (see Fig. 14). It also may be due in part to tone-synchronization mismatches since tone re-synching was not implemented, as noted above.

The second of the static tests, Test 5, was approximately 1 h in duration (about 66 min), and the nominal (planned) P_RNR was 9.2 dB-Hz. Given the low dynamics and somewhat lower P_RNR, the carrier was tracked with the following parameters for Test 5: $T = 15$-s detection interval (carrier estimates output at a 1-Hz rate to facilitate tone demodulation); $\Delta f = 1$-Hz FFT frequency resolution (100,000 frequency cells); and three frequency rates searched, 0 Hz/s and ± 0.05 Hz/s. A plot of the tracked carrier for a segment of Test 5 is provided in Fig. 16. A slow carrier drift again is observed with drift rates varying

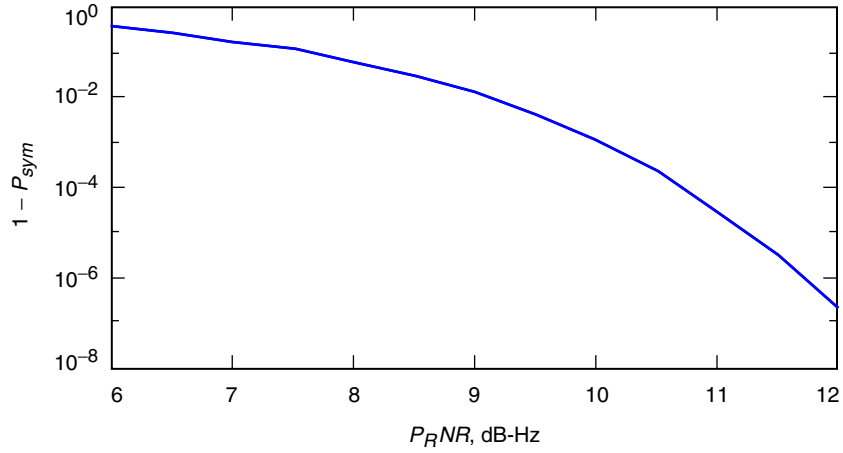

Fig. 15. Theoretical data-tone error probability with $M = T\Delta f = 10$ and $N_{sym} = 256$.

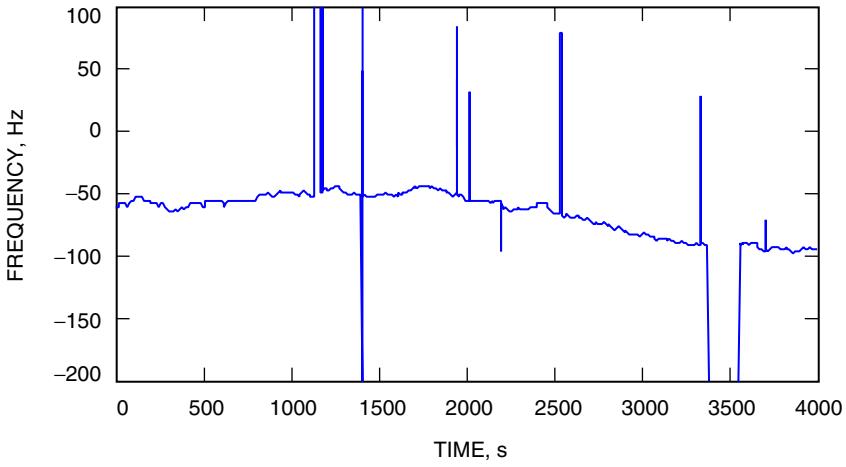

Fig. 16. Carrier-tracking estimates for Test 5.

from 0 to −0.03 Hz/s. These fall well within the frequency-rate search range (±0.05 Hz/s). Based on the average peak carrier amplitudes as well as the average background spectral noise level, the ratio of carrier power-to-noise spectral density CNR was estimated to be approximately 5.5 dB-Hz. This is only 0.2 dB less than the planned $CNR = P_R NR \cdot \cos^2 \Delta \sim 5.7$ dB-Hz. It should be noted that many more carrier-tracking errors occur for Test 5 than for Test 4 (Fig. 14) due to the lower $P_R NR$.

In addition to carrier tracking, the tones also were demodulated using the following parameters: $T = 10$-s detection interval and $\Delta f = 1$-Hz FFT frequency resolution. These parameters correspond to $M = T\Delta f = 10$ in Eq. (11). Furthermore, given that 1 of 256 possible tones was transmitted every 10 s (100-Hz separation between tone frequencies), the search space was restricted to the 256 possible tone locations, i.e., $N_{sym} = 256$ in Eq. (11). The corresponding plot of data-tone error probability $1 - P_{sym}$ versus $P_R NR$ is provided in Fig. 15.

Based on the average detected tone power as well as the average background spectral noise level, the ratio of tone power (in the primary subcarriers)-to-noise spectral density was estimated to be approximately 5.4 dB-Hz. This is about 0.3 dB smaller than the planned $\sin^2 \Delta \cdot P_R NR \cdot 8/\pi^2 \sim 5.7$ dB-Hz. Thus, given the above CNR estimate for Test 5 of 5.5 dB-Hz and the 5.4-dB-Hz estimate for the ratio of tone power-to-noise spectral density, we estimate $P_R NR$ for Test 5 to be approximately 9 dB-Hz—only 0.2 dB lower than planned.

Given the large number of carrier-tracking errors for Test 5, we estimated the tone-error probability with and without the carrier-tracking errors included. Excluding these errors, only 26 out of 363 tones were incorrectly detected, corresponding to a measured tone-error probability of $1 - P_{sym} \sim 0.072$. Including the carrier-tracking errors, approximately 57 out of 396 tones were incorrectly detected, corresponding to a measured tone-error probability of $1 - P_{sym} \sim 0.144$—a doubling of the tone-error rate. With reference to Fig. 15, we see that theoretically a tone-error probability of 0.072 can be achieved at $P_R NR \sim 7.9$ dB-Hz, thus implying an implementation loss of $9 - 7.9 = 1.1$ dB without the carrier-tracking errors. Similarly, a theoretical tone-error probability of 0.144 can be achieved at $P_R NR \sim 7.3$ dB-Hz, thus implying an implementation loss of $9 - 7.3 = 1.7$ dB when carrier-tracking errors are taken into account.

On the other hand, we would theoretically expect a tone-error probability of $1 - P_{sym} \sim 0.0125$ at $P_R NR = 9$ dB-Hz (Fig. 15). Substituting this into Eq. (14) with $N = 363$ (and replacing P_{acq} with P_{sym}), it is seen that the tone-error probability estimate (without carrier-tracking losses, 0.072) falls well outside the standard deviation of the theoretical probability (∼0.0058). Thus, it can be concluded that the 1.1-dB implementation loss in tone-detection performance observed in Test 5 is statistically significant.

B. Selected Processing Results from the Second Series of EDL Tests

We first present the results of carrier-acquisition/tracking tests, Test 2010, when a simulated EDL signal was generated and recorded in complex baseband format at a 100-kHz sample rate. The signal comprised a carrier (periodic frequency variation between approximately ±10 kHz, corresponding to a constant 20-Hz/s^2 frequency acceleration) and 5-s subcarrier data tones. The modulation index was held constant at 48 deg. The 2010 test scenario was similar to Test 8 in the first series of tests except that $P_R NR$ was gradually decreased from nominally 22 dB-Hz to 17 dB-Hz (a 0.5-dB drop every 30 min) for purposes of assessing and comparing carrier-acquisition and tracking thresholds. The test duration of 2010 was approximately 3 h. Wideband (100-kHz-wide) carrier-acquisition and narrowband (400-Hz-wide) tracking over approximately 60 percent of the data set (about 100 min) was carried out with the following carrier-acquisition and tracking parameters used by the EDL processor:

(1) $T = 1$-s detection interval: acquisition and tracking (carrier estimates output at a 2-Hz rate to facilitate tone demodulation and reduce the rate search space)

(2) $\Delta f =$ both 10-Hz and 20-Hz FFT frequency resolution: acquisition and tracking

(3) Frequency search space:

   (a) Acquisition: 5000 frequency cells when $\Delta f = 20$ Hz and 10,000 frequency cells when $\Delta f = 10$ Hz

   (b) Tracking: 21 frequency cells $(400/20 + 1)$ when $\Delta f = 20$ Hz and 41 frequency cells when $\Delta f = 10$ Hz

(4) Frequency rate search space:

   (a) Acquisition: from -800 Hz/s to 800 Hz/s in steps of 25 Hz/s (65 total rates) when $\Delta f = 20$ Hz and rates from -700 Hz/s to 700 Hz/s in steps of 50 Hz/s (29 total rates) when $\Delta f = 10$ Hz

   (b) Tracking: from -20 Hz/s to 20 Hz/s in steps of 5 Hz/s (9 total rates) when $\Delta f = 20$ Hz and rates from -15 Hz/s to 15 Hz/s in steps of 2.5 Hz/s (13 total rates) when $\Delta f = 10$ Hz

Plots of the resulting carrier-frequency estimates are presented in Fig. 17, corresponding to $\Delta f =$ both 10-Hz and 20-Hz FFT resolutions. Superimposed on these plots are the three $P_R NR$ estimates derived as discussed above in connection with the first series tests: Tests 4 and 5. Specifically, over the processed 100-min segment displayed in Fig. 17, the planned/estimated values for $P_R NR$ are as follows:

(1) Segment 1 (10–40 min): $P_R NR = 19$ dB-Hz (planned)/19.3 dB-Hz (estimate)

(2) Segment 2 (40–70 min): $P_R NR = 18.5$ dB-Hz (planned)/18.6 dB-Hz (estimate)

(3) Segment 3 (70–100 min): $P_R NR = 18$ dB-Hz (planned)/18.1 dB-Hz (estimate)

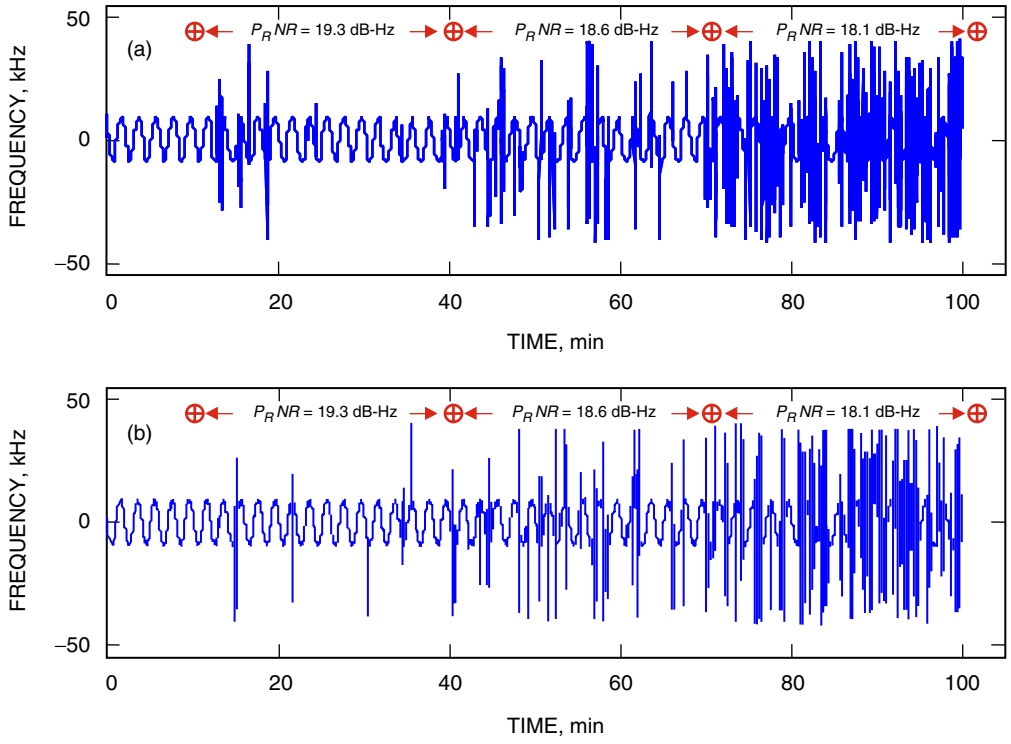

Fig. 17. Carrier acquisition/tracking estimates for Test 2010: (a) Δf = 20-Hz FFT resolution and (b) Δf = 10-Hz FFT resolution.

Thus, the estimates are slightly higher than the planned values. Although not easily discernible, the carrier-tracking performance at $\Delta f = 10$ Hz [Fig. 17(b)] is somewhat better than that at $\Delta f = 20$ Hz [Fig. 17(a)]. However, in either case, tracking performance degrades dramatically once $P_R NR$ falls much below 18.5 dB-Hz.

To better compare the carrier-acquisition and tracking performance, the carrier-tracking error probabilities have been estimated at the above estimated values for $P_R NR$. In estimating the error probability, a 25-min subsegment lying within each constant $P_R NR$ interval first is identified. The error analysis then is restricted to just the time instants when the EDL processor program was in the tracking mode (Fig. 5). Based on the known periodic carrier-frequency curve, the error between the tracked frequency and the known carrier frequency then is computed as a function of time. If this error exceeds at least one or more frequency-resolution interval Δf, then a carrier-tracking error is declared. This error counting is done on a second-by-second basis since a $T = 1$-s detection interval was used to track the carrier.

Plots of the resulting average carrier-tracking error probability are presented in Fig. 18 as a function of $P_R NR$ for both $\Delta f = 20$-Hz [Fig. 18(a)] and 10-Hz [Fig. 18(b)] FFT resolutions. In addition, the theoretical error-probability curves also are included in Fig. 18, corresponding to $\Delta = 48$ deg; $T = 1$ s; $N_f = 9$ rates $\times$ 21 frequency cells $= 189$ when $\Delta f = 20$ Hz; and $N_f = 533$ when $\Delta f = 10$ Hz. As is seen at $\Delta f = 20$ Hz, there is a 1.1-dB implementation loss relative to theoretical performance at a carrier-tracking error probability of approximately 4.4×10^{-2}, which corresponds to the measured error probability at $P_R NR = 19.3$ dB-Hz. At $\Delta f = 10$ Hz, we see that, at the lowest measured tracking-error probability of approximately 2.1×10^{-2} (measured at $P_R NR = 19.3$ dB-Hz), the implementation loss increases by 0.2 dB to 1.3 dB. In both cases, the implementation losses increase as $P_R NR$ decreases

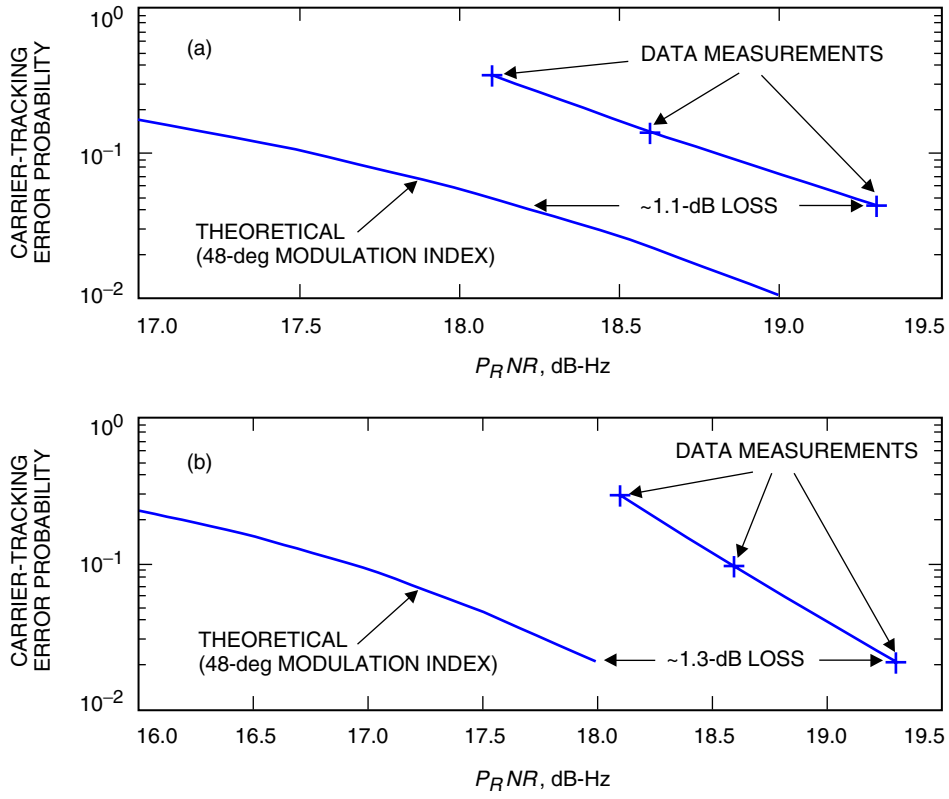

Fig. 18. Carrier-tracking error probabilities for Test 2010: (a) $\Delta f = 20$-Hz FFT resolution and (b) $\Delta f = 10$-Hz FFT resolution.

toward 18 dB-Hz. This is clearly a consequence of the higher carrier-tracking and reacquisition errors that make reliable measurements of tracking-error probabilities virtually impossible at the lower values of $P_R NR$.

In addition to carrier-acquisition testing, two tone-detection tests were conducted under nominally static carrier-frequency conditions (with the exception of slow oscillator drifts) and low $P_R NR$ conditions. For both tests, the signal comprised the carrier and 30-s subcarrier data tones. The modulation index was held constant at 48 deg. The first of these tests, Test 2006, was approximately 90 min in duration and the nominal (planned) $P_R NR$ was 9.5 dB-Hz. Given the low dynamics and low $P_R NR$, the carrier was tracked with the following parameters for Test 2006: $T = 15$-s detection interval (carrier estimates output at a 1-Hz rate to facilitate tone demodulation); $\Delta f = 1$-Hz FFT frequency resolution (100,000 frequency cells); and three frequency rates searched, 0 Hz/s and ± 0.05 Hz/s.

A plot of the tracked carrier for Test 2006 is provided in Fig. 19. A slow carrier drift is observed with drift rates varying from -0.18 to -0.006 Hz/s. These are tracked with the frequency-rate search range (± 0.05 Hz/s). Based on the average peak carrier amplitudes as well as the average background spectral noise level, the ratio of carrier power-to-noise spectral density CNR was estimated to be approximately 6.6 dB-Hz. This is about 0.6 dB larger than the planned $CNR = P_R NR \cdot \cos^2 \Delta \sim 6$ dB-Hz.

In addition to carrier tracking, the tones were also demodulated using the following parameters: both $T = 10$-s (shortened) and 30-s detection intervals and $\Delta f = 1$-Hz FFT frequency resolution. These parameters correspond to $M = T\Delta f = 10, 30$ in Eq. (11). Furthermore, given that 1 of 256 possible tones was transmitted every 10 s (a 100-Hz separation between tone frequencies), the search space was restricted to the 256 possible tone locations, i.e., $N_{sym} = 256$ in Eq. (11). A plot of the (theoretical) data-tone error probability $1 - P_{sym}$ versus $P_R NR$ with $M = 30$ is provided in Fig. 20. Also plotted, for the sake of convenience, is the corresponding error probability with $M = 10$ (from Fig. 15).

Based on the average detected tone power as well as the average background spectral noise level, the ratio of tone power (in the primary subcarriers)-to-noise spectral density was estimated to be approximately 6.8 dB-Hz. This is about 0.8 dB larger than the planned $\sin^2 \Delta \cdot P_R NR \cdot 8/\pi^2 \sim 6$ dB-Hz. Thus, given the above CNR estimate for Test 2006 of 6.6 dB-Hz as well as the 6.8 dB-Hz estimate for the ratio of tone power-to-noise spectral density, we estimate $P_R NR$ for Test 2006 to be approximately 10.1 dB-Hz—0.6 dB higher than planned (analogous to the Round 1, Test 4 results).

Out of a total of 173 transmitted tones in Test 2006, only 2 were incorrectly demodulated when a shortened $T = 10$-s detection interval was used. There were no tone errors when the full $T = 30$-s detection interval was used. Thus, with a $T = 10$-s detection interval, the measured tone-error probability

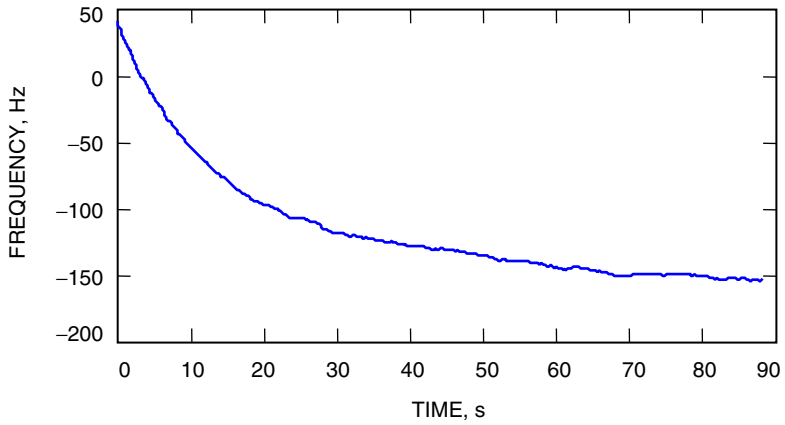

Fig. 19. Carrier-tracking estimates for Test 2006.

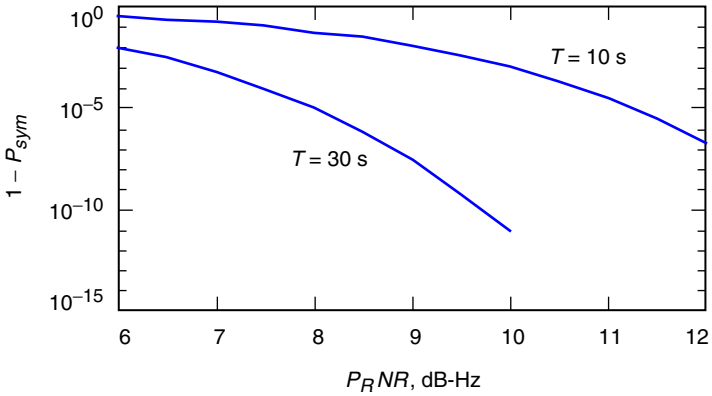

Fig. 20. Theoretical data-tone error probability with $M = T\Delta f = 10, 30$ and $N_{sym} = 256$.

is $1 - P_{sym} = 2/173 \sim 0.011$. With reference to Fig. 20 ($T = 10$ s), we see that theoretically a tone-error probability of 0.011 can be achieved at $P_R NR \sim 9$ dB-Hz, thus implying an implementation loss of $10.1 - 9 = 1.1$ dB.

On the other hand, we would expect theoretically a tone-error probability of $1 - P_{sym} \sim 0.001$ at $P_R NR = 10.1$ dB-Hz (Fig. 20). Substituting this into Eq. (14) with $N = 173$ (and replacing P_{acq} with P_{sym}), it is seen that the tone-error probability estimate (0.011) falls well outside the standard deviation of the theoretical probability ($\sim 2.4 \cdot 10^{-3}$), implying that the 1.1-dB differential between theoretical and measured performance is indeed due to implementation losses. This loss is about one-half that of the Round 1 results for Test 4 at a comparable measured tone-error probability (2.2-dB measured loss). No corresponding conclusions for tone-detection implementation loss can be inferred from the $T = 30$-s detection interval processing results since no tone errors were registered.

The second of the static tests, Test 2007, was also 90 min in duration, and the nominal (planned) $P_R NR$ was 8.5 dB-Hz. Given the low dynamics and somewhat lower $P_R NR$, the carrier was tracked with the following parameters for Test 2007: $T = 20$-s detection interval (carrier estimates output at a 1-Hz rate to facilitate tone demodulation); $\Delta f = 1$-Hz FFT frequency resolution (100,000 frequency cells); and three frequency rates searched, 0 Hz/s and ± 0.05 Hz/s. A plot of the tracked carrier for Test 2007 is provided in Fig. 21. A slow carrier drift again is observed with drift rates varying from 0.01 to -0.005 Hz/s. These fall well within the frequency-rate search range (± 0.05 Hz/s). Based on the average peak carrier amplitudes as well as the average background spectral noise level, the ratio of carrier power-to-noise spectral density CNR was estimated to be approximately 5.6 dB-Hz. This is 0.6 dB larger than the planned $CNR = P_R NR \cdot \cos^2 \Delta \sim 5.0$ dB-Hz.

In addition to carrier tracking, the tones were also demodulated using the following parameters: both $T = 10$-s (shortened) and 30-s detection intervals and $\Delta f = 1$-Hz FFT frequency resolution. These parameters correspond to $M = T\Delta f = 10, 30$ in Eq. (11). Furthermore, given that 1 of 256 possible tones was transmitted every 10 s (a 100-Hz separation between tone frequencies), the search space was restricted to the 256 possible tone locations, i.e., $N_{sym} = 256$ in Eq. (11). The corresponding plots of data-tone error probability $1 - P_{sym}$ versus $P_R NR$ are provided in Fig. 20.

Based on the average detected tone power as well as the average background spectral noise level, the ratio of tone power (in the primary subcarriers)-to-noise spectral density was estimated to be approximately 5.7 dB-Hz. This is about 0.7 dB larger than the planned $\sin^2 \Delta \cdot P_R NR \cdot 8/\pi^2 \sim 5.0$ dB-Hz. Thus, given the above CNR estimate for Test 2007 of 5.6 dB-Hz and the 5.7 dB-Hz estimate for the ratio of tone power-to-noise spectral density, we estimate $P_R NR$ for Test 2007 to be approximately 9.1 dB-Hz—about 0.5 dB higher than planned.

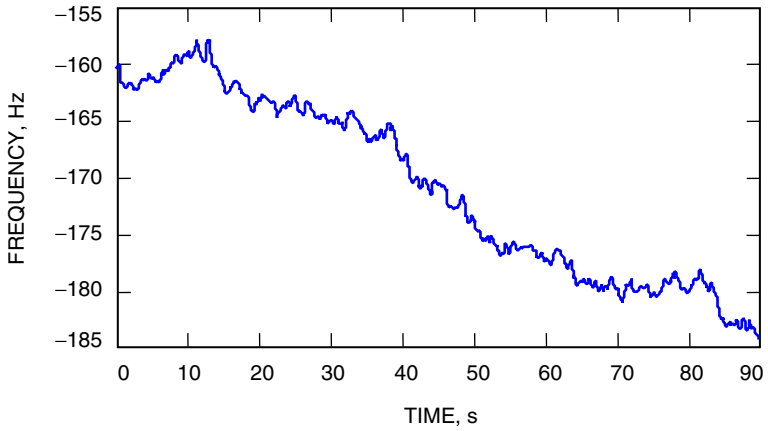

Fig. 21. Carrier-tracking estimates for Test 2007.

Out of a total of 178 transmitted tones in Test 2007, 11 were incorrectly demodulated when a shortened $T = 10$-s detection interval was used. Again, there were no tone errors when the full $T = 30$-s detection interval was used. Thus, with a $T = 10$-s detection interval, the measured tone-error probability is $1 - P_{sym} = 11/178 \sim 0.062$. With reference to Fig. 20 ($T = 10$ s), we see that theoretically a tone-error probability of 0.062 can be achieved at $P_R NR \sim 8$ dB-Hz, thus implying an implementation loss again of $9.1 - 8 = 1.1$ dB.

On the other hand, we would expect theoretically a tone-error probability of $1 - P_{sym} \sim 0.01$ at $P_R NR = 9.1$ dB-Hz (Fig. 20). Substituting this into Eq. (14) with $N = 178$ (and replacing P_{acq} with P_{sym}), it is seen that the tone-error probability estimate (0.062) falls well outside the standard deviation of the theoretical probability ($\sim 7.5 \cdot 10^{-3}$), implying that the 1.1-dB differential between theoretical and measured performance is indeed due to implementation losses. This loss is comparable with that of the Round 1 results for Test 5 at a comparable measured tone-error probability (also a 1.1-dB measured loss). Once again, no corresponding conclusions for tone-detection implementation loss can be inferred from the $T = 30$-s detection interval processing results since no tone errors were registered.

An interesting tone-detection test was conducted, Test 2020P, with approximately 141 transmitted tones, nominally 10 s in duration (for a total test time of about 23 min). However, randomly interspersed with these 10-s tones were 9 special preempted data tones.[21] The durations of these tones were less than 10 s, and from the standpoint of tone-demodulation processing, their presence signaled the onset of a new tone time synch pattern. Consequently, the EDL tone-demodulation scheme previously used was modified to accommodate the randomly changing synchronization pattern employed in Test 2020P. The modification results in a three-pass process wherein hard-tone decisions are first made using only a $T = 1$-s detection interval. A running window then is applied to the 1-s, hard-decision tone data, which determines the greatest number of tone-symbol occurrences in a given window. These data then are used to identify shortened, preempted tones and to correctly demodulate all of the 10-s tones.

Test 2020P was a high $P_R NR$ test (23 dB-Hz planned/23.3 dB-Hz estimated) that used a carrier-frequency profile representative of a typical EDL scenario up to and including the bridle deployment stage. Wideband (100-kHz-wide) carrier-acquisition and narrowband (400-Hz-wide) tracking over the entire data set were carried out with the following carrier-acquisition and tracking parameters used by the EDL processor:

[21] These tones are preempted by tones signaling the onset of special events such as parachute deployment.

(1) T = 1-s detection interval: acquisition and tracking (carrier estimates output at a 2-Hz rate to facilitate tone demodulation and reduce the rate search space)

(2) Δf = 20-Hz FFT frequency resolution: acquisition and tracking

(3) Frequency search space:

  (a) Acquisition: 5000 frequency cells

  (b) Tracking: 21 frequency cells (400/20 + 1)

(4) Frequency rate search space:

  (a) Acquisition: from −800 Hz/s to 800 Hz/s in steps of 25 Hz/s (65 total rates)

  (b) Tracking: from −20 Hz/s to 20 Hz/s in steps of 5 Hz/s (9 total rates)

A plot of the tracked carrier for Test 2020P is provided in Fig. 22. As is seen, the carrier is tracked almost perfectly over the entire 23-min test duration. This is a consequence of the high P_RNR used for this test. The resulting estimated carrier profile was used to demodulate the 2020P tones. Out of the 141 tones transmitted, 7 were incorrectly demodulated. However, 3 of these missed tones were preemptory tones that were out of frequency range (>22 kHz away from the carrier), and thus could not be detected correctly. Three more of the missed detections were preempted tones truncated to less than 5 s in duration (one was 4 s; one was 3 s; and the other was only 2 s). This left 1 full (10-s) tone that was missed due to a timing upset (that subsequently corrected itself).

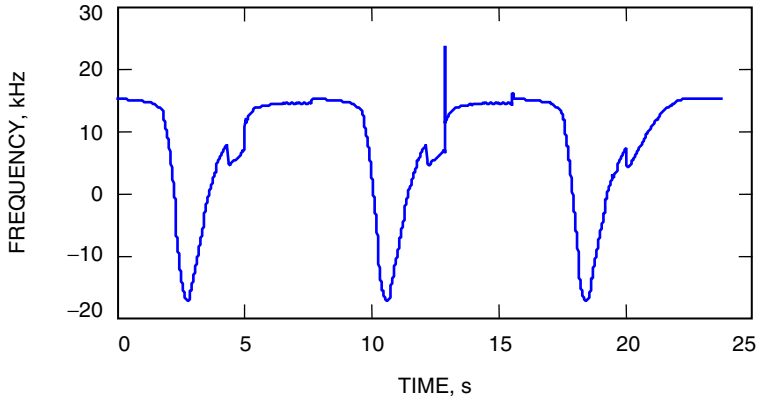

Fig. 22. Carrier-tracking estimates for Test 2020P.

C. Selected Processing Results from the Third Series of EDL Tests

Here we summarize the results of carrier-acquisition/tracking tests, Tests 3011 and 3012, when a simulated EDL signal was generated and recorded in complex baseband format at a 100-kHz sample rate. The signal comprised a carrier (periodic frequency variation between approximately ±10 kHz, corresponding to a constant 20-Hz/s^2 frequency acceleration) and 5-s subcarrier data tones—similar to Test 2010. However, different modulation indices were used for Tests 3011 and 3012. Specifically, the modulation index was held constant at 45 deg for Test 3011 and 40 deg for Test 3012. Like the 2010 test scenario, P_RNR was gradually decreased from nominally 22 dB-Hz to 17 dB-Hz (a 0.5-dB drop every 20 min) for Test 3011 and from 21.5 dB-Hz to 16.5 dB-Hz for Test 3012 (a 0.5-dB drop every 15 min). The duration of Test 3011 was approximately 100 min and that of Test 3012 was 80 min. Wideband (100 kHz-wide) carrier-acquisition and narrowband (400-Hz-wide) tracking were carried out with the following carrier-acquisition and tracking parameters used by the EDL processor for both Tests 3011 and 3012:

(1) T = 1-s detection interval: acquisition and tracking (carrier estimates output at a 2-Hz rate to facilitate tone demodulation and reduce the rate search space)

(2) Δf = 10-Hz FFT frequency resolution: acquisition and tracking

(3) Frequency search space:

  (a) Acquisition: 10,000 frequency cells

  (b) Tracking: 41 frequency cells $(400/10 + 1)$

(4) Frequency rate search space:

  (a) Acquisition: from -700 Hz/s to 700 Hz/s in steps of 50 Hz/s (29 total rates)

  (b) Tracking: from -15 Hz/s to 15 Hz/s in steps of 2.5 Hz/s (13 total rates)

Plots of the resulting carrier-frequency estimates are presented in Fig. 23, corresponding to both Tests 3011 and 3012. Superimposed on these plots are the corresponding P_RNR estimates. Over the processed segments displayed in Fig. 23, the planned/estimated values for P_RNR are as follows:

3011, Segment 1 (8–27 min): $P_RNR = 19$ dB-Hz (planned)/18.7 dB-Hz (estimate)

3011, Segment 2 (27–47 min): $P_RNR = 18.5$ dB-Hz (planned)/18.4 dB-Hz (estimate)

3011, Segment 3 (47–67 min): $P_RNR = 18$ dB-Hz (planned)/17.8 dB-Hz (estimate)

3011, Segment 4 (67–87 min): $P_RNR = 17.5$ dB-Hz (planned)/could not estimate

3012, Segment 1 (8–19 min): $P_RNR = 18.5$ dB-Hz (planned)/18 dB-Hz (estimate)

3012, Segment 2 (19–34 min): $P_RNR = 18$ dB-Hz (planned)/17.5 dB-Hz (estimate)

3012, Segment 3 (34–49 min): $P_RNR = 17.5$ dB-Hz (planned)/17 dB-Hz (estimate)

3012, Segment 4 (49–64 min): $P_RNR = 17$ dB-Hz (planned)/could not estimate

Thus, the estimates are generally lower than the planned values. In fact, the constant 0.5-dB difference between the planned and estimated P_RNR values for Test 3012 suggests that the attenuator might have been set 0.5 dB lower than planned for this test. The carrier estimates obtained for Test 3012 are clearly superior to those for Test 3011 due to the smaller modulation index (40 deg) used in generating the Test 3012 data. For Test 3011, carrier-tracking performance degrades dramatically once P_RNR falls below 17.8 dB-Hz, and for Test 3012 this occurs once P_RNR falls much below 17 dB-Hz.

To better compare the carrier-acquisition and tracking performance, the carrier-tracking error probabilities have been estimated at the above estimated values for P_RNR (analogous to the analysis performed for Test 2010—see Fig. 18). Plots of the resulting average carrier-tracking error probability are presented in Fig. 24 as a function of P_RNR for both Tests 3011 and 3012. In addition, the theoretical error-probability curves are also included in Fig. 24, corresponding to $T = 1$ s; $N_f = 533$; and $\Delta = 45$ deg (Test 3011) or $\Delta = 40$ deg (Test 3012).

As is seen for both tests, the implementation loss is about 1.5 dB relative to theoretical performance at a carrier-tracking error probability of approximately 3×10^{-2}, which corresponds to the measured error probability at $P_RNR = 18.7$ dB-Hz in the case of Test 3011 or at $P_RNR = 18$ dB-Hz in the case of Test 3012. Again we note that the implementation losses increase as P_RNR decreases. This is clearly a consequence of the higher carrier-tracking and reacquisition errors, which make reliable measurements of tracking-error probabilities virtually impossible at the lower values of P_RNR.

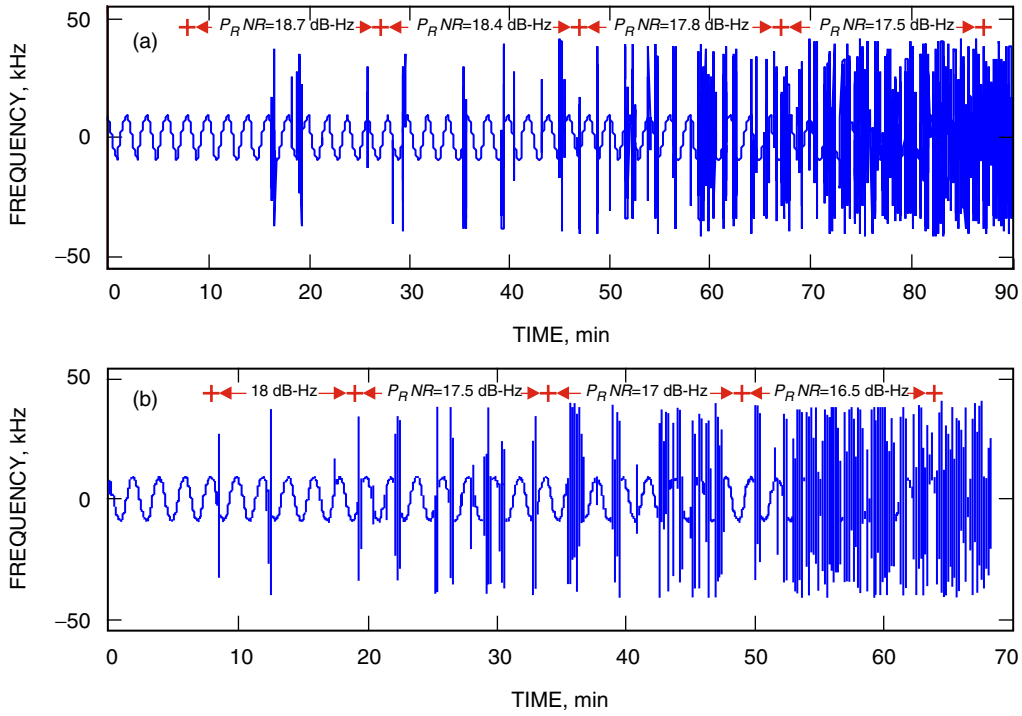

Fig. 23. Carrier acquisition/tracking estimates for Tests (a) 3011 and (b) 3012. The $P_R NR$ values indicated for the 4th segments are extrapolated from the planned values and estimates.

Finally, in Fig. 25, we compare the carrier-tracking error probabilities for Test 2010 ($\Delta = 48$ deg and $\Delta f = 10$-Hz FFT frequency resolution); Test 3011 ($\Delta = 45$ deg); and Test 3012 ($\Delta = 40$ deg). As is seen, there is about a 0.3-dB differential between the 3011 and 2010 measurement curves and a 0.75-dB differential between the 3012 and 3011 measurement curves. These differentials approximately correspond to the power differences between the three different modulation indices, i.e.,

$$20 \cdot \log 10 \left\{ \frac{\cos(45°)}{\cos(48°)} \right\} \sim 0.5 \text{ dB}$$

and

$$20 \cdot \log 10 \left\{ \frac{\cos(40°)}{\cos(45°)} \right\} \sim 0.7 \text{ dB}$$

Based on the theoretical results presented in Section IV, it was shown (Fig. 7) that a smaller modulation index ($\Delta \sim 40$ to 45 deg) is desirable from the standpoint of carrier acquisition. The experimental results presented in this section (Fig. 25) also support a smaller modulation index from the standpoint of carrier tracking. Furthermore, extrapolating the Test 2010 tracking-error measurements down to 0.01 (Fig. 25) suggests a carrier-tracking threshold at $P_R NR \sim 19.5$ dB-Hz when $\Delta = 48$ deg. Reducing this by 0.3 dB implies a carrier-tracking threshold at 19.2 dB-Hz when $\Delta = 45$ deg, and reducing by another 0.75 dB implies a carrier-tracking threshold at approximately 18.5 dB-Hz when $\Delta = 40$ deg. In all cases, tone detectability is well above 99 percent—even taking into account a 1- to 2-dB implementation loss (see Fig. 9). Consequently, we conclude that a modulation index between 40 and 45 deg should be used during periods of highest dynamics (at least through bridle swinging—see Fig. 1) and that this be increased to 48 deg after landing.

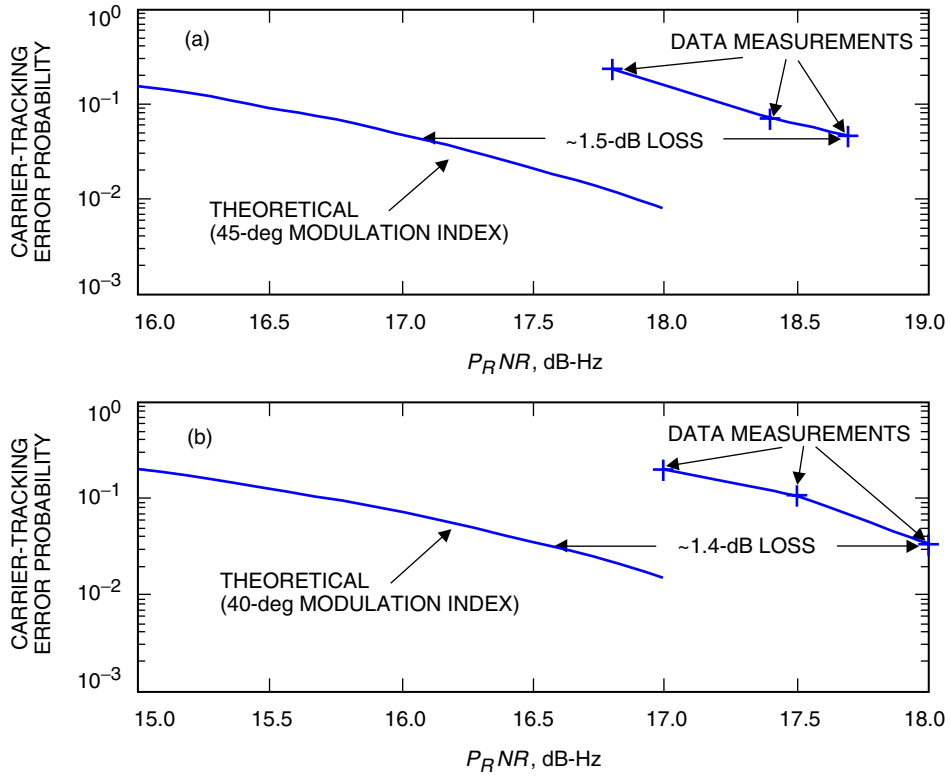

Fig. 24. Carrier-tracking error probabilities for Tests: (a) 3011 and (b) 3012.

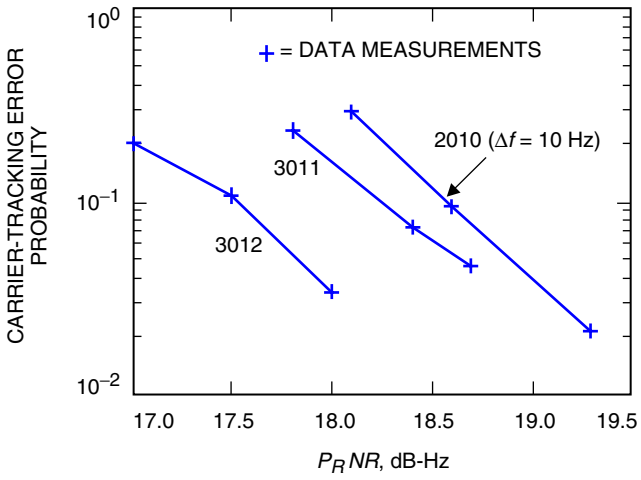

Fig. 25. Carrier-tracking error probabilities for Tests 2010, 3011, and 3012.

VI. Conclusions

A special form of 256-tone MFSK modulation will be used to communicate from the MER spacecraft to Earth during the challenging EDL phase of the mission. The residual-carrier component of the signal will be acquired and tracked using FFT-based algorithms. The algorithms detect the signal and estimate frequency and frequency rate by maximizing a detection function over these parameters. This technique enables frequency tracking at an SNR approximately 6 dB lower than would permit coherent tracking with a phase-locked loop, under the same dynamics conditions. After tracking the carrier frequency, the MFSK tones are detected using similar processing. It has been shown that the modulation scheme and processing algorithms will be capable of reliable communication to Earth throughout most of the EDL phase.

In particular, detailed theoretical and simulation analyses presented in Sections IV and V (see, e.g., Figs. 10, 18, and 24) have shown that reliable carrier tracking at $P_R NR \sim 19.5$ dB-Hz and lower, depending upon the modulation index, is feasible under simulated carrier-frequency dynamics that model the EDL scenario up to parachute deployment. The results of an extensive measurement campaign as summarized in Section V essentially corroborate the theoretical findings. Furthermore, the experimental data provide very useful estimates of losses that can be expected in the field. Specifically, typical losses in carrier-acquisition performance are anticipated to be approximately 1 dB based on the analysis of Test 8 from the first series of EDL experiments (Section V.A, Fig. 11). Carrier-tracking losses range from 1.1 dB (Test 2010, Fig. 18) to 1.5 dB (Tests 3011 and 2012, Fig. 24). Data-tone detection losses range from 1.1 dB (Tests 5, 2006, and 2007) to 2.2 dB (Test 4).

Other issues addressed in this analysis include the accommodation of preempted tones as well as the influence of the modulation index on the carrier-acquisition, tracking, and tone-detection performance. Based on limited experimental measurements as summarized in Section V.C, it is concluded that splitting the power between the carrier and the primary data subcarriers ($\Delta = 48$ deg) is a reasonable strategy after landing, but during periods of highest dynamics (at least through bridle swinging), a smaller modulation index between 40 and 45 deg is desirable. It is anticipated that the design rules developed in this article will provide a basis for creating and modifying the operational configuration files during EDL.[22]

References

[1] W. Hurd, P. Estabrook, C. Racho, and E. Satorius, "Critical Spacecraft-to-Earth Communications for Mars Exploration Rover (MER) Entry, Descent and Landing," *Proceedings of the 2002 IEEE Aerospace Conference,* Big Sky, Montana, pp. 3-1283–3-1292, March 9–16, 2002.

[2] G. E. Wood, S. W. Asmar, T. A. Rebold, and R. A. Lee, "Mars Pathfinder Entry, Descent, and Landing Communications," *The Telecommunications and Data Acquisition Progress Report 42-131, July–September 1997,* Jet Propulsion Laboratory, Pasadena, California, pp. 1–19, November 15, 1997. http://tmo.jpl.nasa.gov/tmo/progress_report/42-131/131I.pdf

[3] S. Aguirre and W. J. Hurd, "Design and Performance of Sampled Data Loops for Subcarrier and Carrier Tracking," *The Telecommunications and Data Acquisition Progress Report 42-79, July–September 1984,* Jet Propulsion Laboratory, Pasadena, California, pp. 81–95, November 15, 1984. http://tmo.jpl.nasa.gov/tmo/progress_report/42-79/79H.PDF

[22] T. Pham and D. Fort, op cit.

[4] D. D. Morabito, "The Spacecraft Communications Blackout Problem Encountered During Passage or Entry of Planetary Atmospheres," *The Interplanetary Network Progress Report 42-150, April–June 2002,* Jet Propulsion Laboratory, Pasadena, California, pp. 1–23, August 15, 2002.
http://ipnpr.jpl.nasa.gov/progress_report/42-150/150C.pdf

[5] V. Vilnrotter, S. Hinedi, and R. Kumar, "Frequency Estimation Techniques for High Dynamic Trajectories," *IEEE Trans. AES,* vol. 25, no. 4, pp. 559–577, July 1989.

[6] D. J. Torrieri, *Principles of Military Communication Systems,* Chapter 4, Dedham, Massachusetts: Artech House, 1981.

[7] G. Lanyi and R. Kahn, "Tone Detection Via Incoherent Averaging of Fourier Transforms to Support the Automated Spacecraft-Monitoring Concept," *The Telecommunications and Data Acquisition Progress Report 42-129, January–March 1997,* Jet Propulsion Laboratory, Pasadena, California, pp. 1–22, May 15, 1997.
http://tmo.jpl.nasa.gov/tmo/progress_report/42-129/129E.pdf